Available online at www.sciencedirect.com
SCIENCE DIRECT
Precambrian Research 148 (2006) 45–66
Precambrian Research
www.elsevier.com/locate/precamres

The genesis of Archaean chromitites from the Nuasahi and Sukinda massifs in the Singhbhum Craton, India

Sisir K. Mondal [a,*], Edward M. Ripley [b], Chusi Li [b], Robert Frei [c]

[a] *Department of Earth and Planetary Sciences, American Museum of Natural History, New York, NY 10024, USA*
[b] *Department of Geological Sciences, Indiana University, Bloomington, IN 47405, USA*
[c] *Geological Institute, University of Copenhagen, Øster Voldgade 10, DK-1350 Copenhagen, Denmark*

Received 15 March 2005; received in revised form 30 March 2006; accepted 3 April 2006

Abstract

The chromitite deposits of the Nuasahi and Sukinda massifs are part of layered ultramafic bodies which occur within Archaean low-grade metamorphic rocks of the Iron Ore Group (IOG) in the Singhbhum Craton of the Indian Shield. The chromitite seams are interlayered with dunite, and associated with orthopyroxenite. Detailed electron microprobe study reveals very high *Mg*-numbers (0.66–0.82) and *Cr*-numbers (0.75–0.87) for chromite in massive chromitite from the seams, high Fo content ($Fo_{92–95}$) for olivine in dunite and high En content ($En_{89–94}$) for orthopyroxene in orthopyroxenite. Our study suggests that the original igneous compositions for these minerals are preserved in the respective monomineralic rocks and can be used to evaluate the primary magmatic petrogenesis of the rocks. The primitive compositions of the minerals in monomineralic rocks suggest high degree of partial melting of the source mantle during the Mesoarchaean. The parental magma from which the massive chromitites crystallized was of siliceous high-Mg basaltic or boninitic compositions, similar to the compositions of spatially associated chromite-bearing siliceous high-Mg basalts of the Iron Ore Group. The parental magma may have generated due to the interaction of a depleted mantle with a fluid-enriched melt possibly derived in response to the dehydration of a subducting slab. Monomineralic chromitite layers formed either in response to mixing of magmas or due to the suppression of silicate mineral crystallization in response to elevated H_2O concentrations in the parent magmas. The parental magmas that produced chromitites may have intruded into the volcano-sedimentary greenstone belts of a supra-subduction zone setting.

Keywords: Chromite; Chromitite; Peridotite; Subduction; Boninite; Archaean; Nuasahi (Boula); Sukinda; Singhbhum Craton; India

1. Introduction

Massive chromitites are found in a variety of mafic-ultramafic complexes of different tectonic settings. Stratiform chromitite layers occur in large layered intrusions such as the Bushveld and Stillwater Complexes, and in the crustal cumulate portions of ophiolite complexes. Discordant chromitite bodies are found in the lower portions of ophiolites that are thought to represent formation in the upper mantle. Archaean chromite deposits and the associated ultramafic-mafic rocks are found in different geological environments (e.g. Stowe, 1994) and are compositionally distinctive, suggesting derivation from various parental magma types (Rollinson, 1995a). Archaean chromite deposits are commonly found as either stratiform bodies that are interlayered with anorthosite in tonalite gneiss terrane (e.g. Fiskenasset layered intrusion in southern West Greenland, Rollinson et al., 2002),

* Corresponding author. Tel.: +1 11 212 769 5459; fax: +1 11 212 769 5339.
E-mail addresses: smondal@amnh.org, sisir.mondal@gmail.com (S.K. Mondal).

0301-9268/$ – see front matter © 2006 Elsevier B.V. All rights reserved.
doi:10.1016/j.precamres.2006.04.001

or as deformed bodies hosted by serpentinized peridotites in greenstone belts (e.g. Shurugwi greenstone belt in Zimbabwe, Stowe, 1997). One of the principal controls on chromite chemistry is parental melt compositions that vary in different tectonic settings, consequently chromite is a good indicator of the magmatic environment (e.g. Irvine, 1967; Dick and Bullen, 1984; Roeder, 1994; Kamenetsky et al., 2001). However, the compositions of chromite can be modified during cooling at the subsolidus stage and during metamorphism (e.g. Irvine, 1967; Jackson, 1969; Evans and Frost, 1975; Eales and Reynolds, 1986; Barnes, 2000). Therefore, petrological inferences based on chromite compositions require that the liquidus chromite composition be recovered (Rollinson, 1995b). In this paper we utilize primary chromite compositions to evaluate parent magma compositions and infer the tectonic setting of the Archaean chromitites in eastern India.

The Singhbhum Craton in eastern India is one of four significant cratonic nuclei in the Indian Shield (Fig. 1) (Radhakrishna and Naqvi, 1986; Saha, 1994), which contains several chromitite-bearing layered ultramafic bodies within Archaean greenstone belts (Acharyya, 1993; Mondal et al., 2002). The ultramafic rocks are found within supracrustal rocks of the Iron Ore Group mainly in the Nuasahi and Sukinda areas of Orissa state and the Roro-Jojohatu area of Bihar state (Srinivasachari, 1974; Mukhopadhyay and Dutta, 1983; Basu et al., 1997). Previous researchers interpreted the chromite deposits in the Nuasahi and Sukinda massifs either to be cumulates similar to those in large layered complexes such as the Bushveld Complex or mantle rocks similar to those in Alpine type peridotites or ophiolites (e.g. Banerjee, 1972; Chakraborty and Chakraborty, 1984; Page et al., 1985; Varma, 1986; Pal and Mitra, 2004). However, these studies were based on limited chromite and platinum-group element (PGE) data, and questions still remain with respect to origin of the chromitites and their host rocks, their tectonic settings and their broader significance with respect to Archaean crustal evolution. The Nuasahi and Sukinda massifs are of particular interest because they are the most significant chromite-bearing ultramafic bodies of the Archaean greenstone belts in the Indian Shield. The chromite ores account for ≈98% of the total resources in India and ≈2.5% of world resources. The chromitite bodies can be traced for several kilometers along strike and are well exposed in open-cut and underground workings. In addition, gabbro-breccia hosted PGE-mineralization is found in association with chromites in both the Nuasahi and Sukinda massifs. A better understanding of the tectonic setting in which the chromitites formed will be particularly valuable for future platinum exploration in the Archaean greenstone belts.

2. Regional geology

The four Archaean cratonic nuclei of the Indian Shield are the Dharwar, Bastar, and Singhbhum Cratons in the southern block and the Bundelkhand Craton in the northern block (Fig. 1, inset). The eastern part of the Indian Shield is known as the Singhbhum-North Orissa Province (Mukhopadhyay, 1988; Saha, 1994) and is composed of a high-grade metamorphic terrain known as the Chhotanagpur Craton to the north and a granite-greenstone terrain known as the Singhbhum Craton to the south (Fig. 1). The latter consists principally of (1) supracrustal rocks of the Older Metamorphic Group (OMG), and tonalitic rocks of the Older Metamorphic Tonalitic Gneiss (OMTG), (2) several granitoid batholiths (e.g. Singhbhum granite, Nilgiri granite, Bonai granite, Mayurbhanj granite), and (3) supracrustal rocks of the Iron Ore Group (IOG) greenstone sequences (Fig. 1; Table 1).

The Singhbhum Craton has a complex history of tectonic evolution through repeated extension and compression associated with sedimentation and magmatism from early Archaean to Proterozoic (Saha, 1994; Majumder et al., 2000). The Singhbhum Craton is bounded to the north by the Singhbhum shear zone (200 km long) and by the Sukinda thrust to the south. The Singhbhum granite is the largest composite batholith in the craton and has been divided into two phases: Granite of 'Type A' revealed a zircon U–Pb date of 3328 Ma (Mishra et al., 1999), whereas, Granite of 'Type B' has been dated at 3100 Ma by the Pb–Pb whole-rock isochron method (Saha, 1994). The oldest supracrustal suite in the Singhbhum Craton is the OMG with a zircon U–Pb age of 3.5 Ga (Mishra et al., 1999). The OMG consists of meta-igneous and metasedimentary rocks of amphibolite facies. It occurs as remnants along with the OMTG (zircon U–Pb date of 3.44 Ga; Mishra et al., 1999) within the granitic batholithic complex. A Sm–Nd whole-rock isochron age for the orthoamphibolites of the OMG yields an age of 3305 ± 60 Ma, which is considered to be the crystallization age of the protoliths (Sharma et al., 1994). The Archaean terrain experienced extensive mafic-ultramafic magmatism during the Proterozoic within the mobile belts (Fig. 1) such as the Dalma, Dhanjori, Simlipal, Jagannathpur and Malangtoli belts (Mukhopadhyay, 2001). A dolerite dyke swarm (Newer Dolerite, Table 1) intruded the Singhbhum Craton between 2500 and 950 Ma (Saha, 1994; Roy et al., 2005).

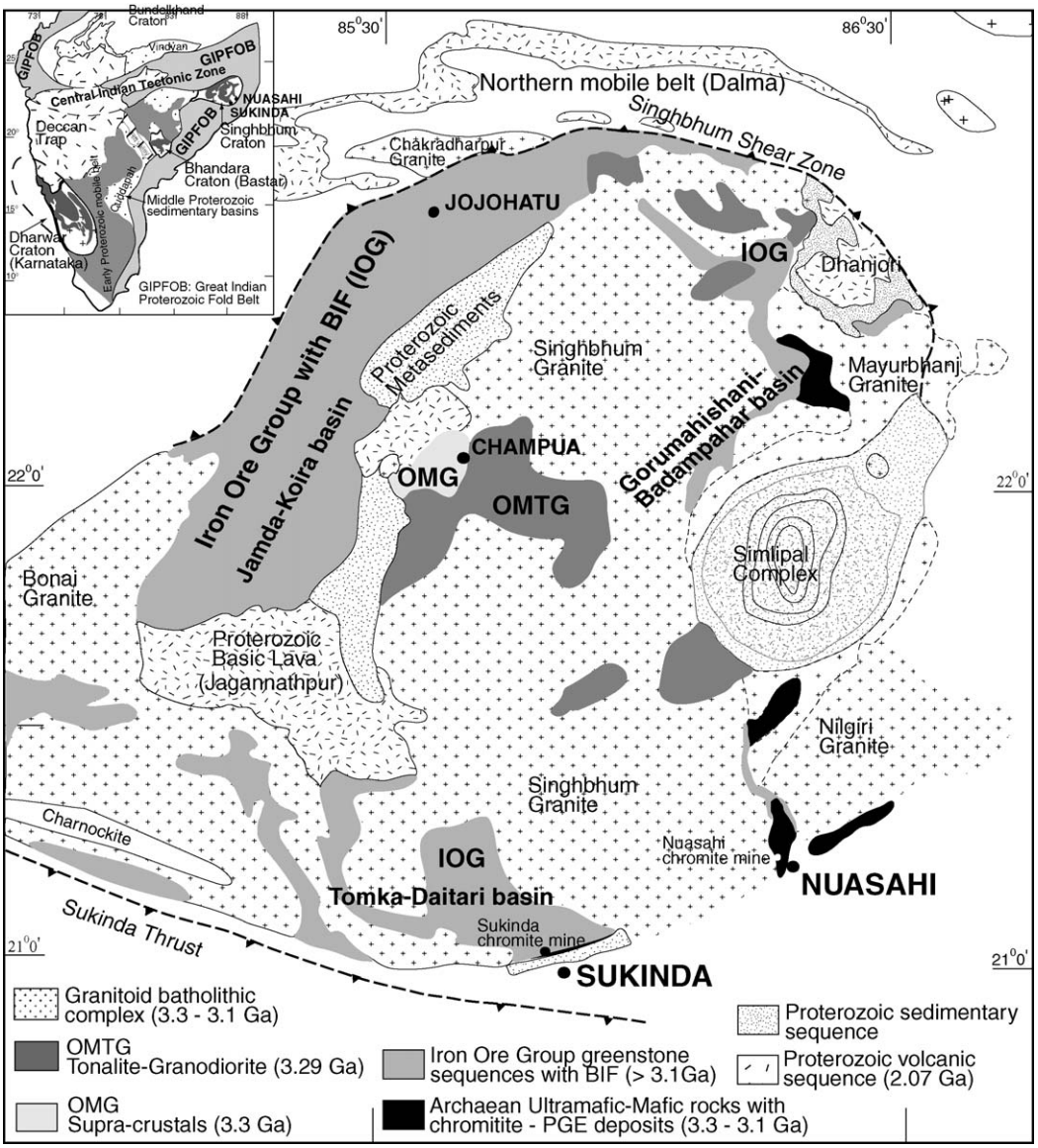

Fig. 1. Geology of the Singhbhum Craton, India (after Saha, 1994; Sengupta et al., 1997). Inset map shows generalized geology of the Indian Shield with locations of the Nuasahi and Sukinda massifs (after Radhakrishna and Naqvi, 1986; Leelananadam et al., 2006).

The IOG greenstone sequences contain Banded Iron Formation surrounding the Singhbhum granitic batholith (Fig. 1). These sequences were developed after the emplacement of the 'Type A' Singhbhum granite batholith. The age of the IOG supracrustal sequences is considered to range between those of the evolutionary stages of the Singhbhum granite (Saha, 1994) i.e. between 3.3 and 3.1 Ga. The IOG greenstone sequences are present mainly in three sedimentary basins (Fig. 1): (1) the Gorumahishani-Badampahar basin in the east, (2) the Jamda-Koira basin in the west, and (3) the Tomka–Daitari basin in the south. The ultramafic rocks of the IOG are in general metamorphosed to lower greenschist to amphibolite facies and consists of schistose aggregate of tremolite, actinolite and chlorite.

The major mafic-ultramafic intrusive bodies (IOG mafic-ultramafic intrusive suite) occur along the southern and eastern parts of the Singhbhum Craton (Fig. 1). The ultramafic suite were emplaced along the marginal fractures in the supracrustal rocks of the IOG greenstone sequences and subsequent to emplacement these were regionally folded with the IOG rock and intruded by granites (Banerjee, 1972). Extensive strike-slip faults, shears and fractures are present within

Table 1
Chronostratigraphy of Singhbhum Craton (after Saha, 1994; Augé et al., 2003)

	Generalized sequence	Zircon ages	Other methods
	Kolhan Group		2100–2200 Ma[a]
Unconformity			
Dolerite dyke swarms	Newer Dolerite Suite		950–2500 Ma[a,b]
Dhanjori-Simlipal-Dalma-Jagannathpur-Malangtoli belts: PMB Igneous Suites; PMB Sedimentary Sequences	Proterozoic Mobile Belt (PMB)		2072 Ma[c]
Metasediments with mafic sills	Singhbhum Group		2300–2400 Ma[a]
Unconformity			
Mayurbhanj Granite	SBG-B	3.1 Ga[d]	
Singhbhum Granite Type B	SBG-B		3.1 Ga[a]
Iron Ore Group igneous and sedimentary sequences: IOG Igneous Suites (Ultramafic-mafic plutonic suite e.g., Nuasahi Sukinda-Jojuhatu-ultramafic suite; gabbro-anorthosite-diorite-mafic suite; Ultramafic-mafic volcanic suite e.g., komatiites and high-Mg basalts in Gorumahishani-Badampahar, Tomaka-Dairai and Jamda-Koira belts; Felsic volcanics); IOG Sedimentary Sequences	Iron Ore Group (IOG)	3121 ± 3 Ma[e] age of zircon from gabbroic suite, Nuasahi breccia zone	3205 ± 280 Ma[e] Sm-Nd isochron age of gabbroic suite from the Nuasahi massif
Singhbhum Granite Type A	SBG-A	3328 ± 7 Ma[d]	3.3 Ga[a]
Older Metamorphic Tonalite Gneiss	OMTG	Age clustering at 3.4 and 3.2 Ga[d]	3288 ± 35 Ma[f] Sm–Nd isochron age with OMG
Older Metamorphic Group	OMG	Age clustering at 3.55, 3.4 and 3.2 Ga[d]	3305 ± 60 Ma[f] Sm–Nd isochron age

[a] Saha et al. (1988).
[b] Roy et al. (2005).
[c] Roy et al. (2002).
[d] Mishra et al. (1999).
[e] Augé et al. (2003).
[f] Sharma et al. (1994).

the steeply dipping ultramafic sequences in both the Sukinda and Nuasahi areas. The ultramafic rocks in these massifs display strong tectonic fabrics, which are superimposed on primary igneous layering. In the Nuasahi area, both the quartzite and phyllite of the IOG have bedding parallel foliation that dips 55–85° towards the southeast or east-southeast. A relatively weak, but consistent, foliation nearly parallel to litho contacts and compositional banding, particularly in extensively serpentinized peridotites, is found in the ultramafic suite of the Nuasahi massif (Mondal, 2000). The ultramafic bodies contain nearly subvertical lensoid and banded chromitite ore bodies. In the Nuasahi area the ultramafic bodies are associated with a large mafic suite. The mafic suite intruded the IOG quartzite as well as the ultramafic suite (Haldar, 1967; Mondal et al., 2001). In the Sukinda area, the mafic suite is also intrusive into the ultramafic suite (Banerjee, 1972) but exposure is limited. The mafic bodies in the Singhbhum Craton are in places intrusive into the 'Type A' Singhbhum granite (3.3 Ga) but are also intruded by some granophyric rocks that are thought to be equivalent to the Mayurbhanj granite of 3.1 Ga age (Saha, 1994). Augé et al. (2003) obtained U–Pb zircon ages of 3123 ± 7 and 3119 ± 6 Ma for the gabbroic matrix of the PGE-mineralized breccia zone in the Nuasahi massif that were described by Mondal and Baidya (1997), Mondal (2000) and Mondal et al. (2001). Sm–Nd whole-rock isotopic measurements of the gabbroic samples define an isochron corresponding to an age of 3205 ± 280 Ma (Augé et al., 2003). The absolute age of the ultramafic plutonic bodies has not yet been determined. However, field relations and available ages for the associated rocks suggest possible age limits between 3.3 and 3.1 Ga for the chromitite-bearing ultramafic suite of the Nuasahi and Sukinda massifs. The ultramafic plutonic bodies of the Nuasahi and Sukinda massifs show

extensive hydrothermal alteration, but original unaltered igneous cumulate textures are still preserved. A chlorite-amphibole rich assemblage is commonly developed in the altered gabbroic rocks of the mafic suite. However, no metamorphic fabric is developed in the gabbroic suite.

3. Geologic setting of the chromite deposits

The ultramafic-mafic bodies of the Nuasahi massif occupy an area of nearly 10 sq. km and occur at the south-eastern part of the Singhbhum Craton (Figs. 1 and 2a, inset). Immediate country rocks belong to the Iron Ore Group. Ghosh and Prasada Rao (1952) first described the geology of the area and observed that the chromitite-bearing ultramafic rocks occur as bands, that are surrounded by gabbro. Haldar (1967) demonstrated that the gabbroic suite intruded the chromitite-bearing ultramafic suite after the faulting and shearing of the ultramafic suite and concluded that the ultramafic and gabbroic suites in the Nuasahi area were formed through successive intrusions in distinctly different periods and environments.

Mondal et al. (2001) divided the Nuasahi massif into three magmatic suites. Suite 1 consists of a steeply dipping interlayered sequence of chromitite-bearing ultramafic rocks (Fig. 2a). These rocks are exposed in an area of ∼5 km in length and up to 400 m width, with a general NW-SE to NNW-SSE trend. Igneous layering in these rocks generally dips between 60° and 80° towards the northeast and east. Three differently trending major fault zones (NNW-SSE, NE-SW and ENE-WSW) are present within the ultramafic belt, and at least five major segments formed due to intense faulting. The individual segments of the ultramafic belt are 500–1000 m long and 300–450 m wide. The major NE-SW trending boundary fault at the northwestern part of the massif has separated the quartzites of the IOG from the ultramafic belt (Fig. 2a, inset). The ultramafic belt (Suite 1) consists of orthopyroxenite (enstatitite), harzburgite, dunite and chromitite. Dunite is a major lithologic unit and is nearly 130–150 m thick. Three major dismembered chromitite seams are present and hosted in dunite, which are named by the local mining authorities as Durga, Laxmi 2 and Laxmi 1 (from west to east in the belt, Fig. 2a and Section 3). The contacts between the chromitite seams and their host dunite are mostly faulted and sheared, but locally original gradational contacts are also found. The dunite unit is flanked by orthopyroxenite. The contact between dunite and orthopyroxenite is sharp but not of an intrusive nature. The orthopyroxenite unit to the east of the dunite unit is ∼80–120 m thick and intensely brecciated along the hanging wall portions. The orthopyroxenite unit to the west of the dunite unit is coarser in grain size than the eastern orthopyroxenite unit. Remnants of harzburgite are present in the western orthopyroxenite near the dunite unit. A number of magnesite veins and veinlets have transgressed the serpentinized ultramafic suite. Suite 2 is composed of gabbroic rocks with intrusive bands and lenses of titaniferous magnetite. The rocks include pyroxenite, norite, gabbro, anorthosite and grade into dioritic rocks in the northeastern part of the massif (Fig. 2a). The gabbroic rocks at the eastern part of the ultramafic belt are hybrid in character and strongly altered due to hydrothermal processes. Suite 3 consists of later intrusive phases such as dolerite, clinopyroxenite, pegmatitic gabbro and quartz-diorite.

The largest ultramafic body in the Singhbhum Craton is the Sukinda massif (∼25 km × ∼400 m, Fig. 2b). Exposures of the rocks in the Sukinda massif are poor because of the extensive deep leteritic weathering. Basu et al. (1997) described the geology of the area based on drill core data and reported that the Sukinda massif comprises a package of extrusive metabasalts and intrusive ultramafic rocks, which occur as a part of the folded sequences of the IOG. The ultramafic belt forms a southwesterly plunging synform with a moderately dipping north limb (40–50°) and subvertical south limb (Banerjee, 1972). The ultramafic rocks are covered by thick soil and laterite (often up to 30 m thick) and weathered profile of sapprolitic and limonitic rocks. Two major horizons of metabasalts are present, one at the base of the ultramafic body in the east, and another at the synformal core in the west. The contact between the ultramafic and lower metabasalt appears to be highly fractured and brecciated (Basu et al., 1997). The chromitite bands and lenses occur within serpentinized dunite. The orthopyroxenite is relatively unaltered and has a sharp contact with the serpentinized dunite. In the western part of the Sukinda massif chromitite bodies are extensively deformed and fragmented, and impregnated by gabbroic rock (Fig. 2b). Sarkar et al. (2001) described a breccia zone from this area, which is similar to that found in the Nuasahi massif as documented by Mondal and coworkers (e.g. Mondal and Baidya, 1997).

4. Description of rocks

4.1. Chromitites

The chromitite seams within the ultramafic belt of the Nuasahi massif are currently being mined for chromium ore, with reserves estimated to occur to depth of 280 m. The chromitite seams are steeply dipping (nearly subvertical) and occur as dissected bands and as elongated lenses. The Durga chromitite seam is the western most

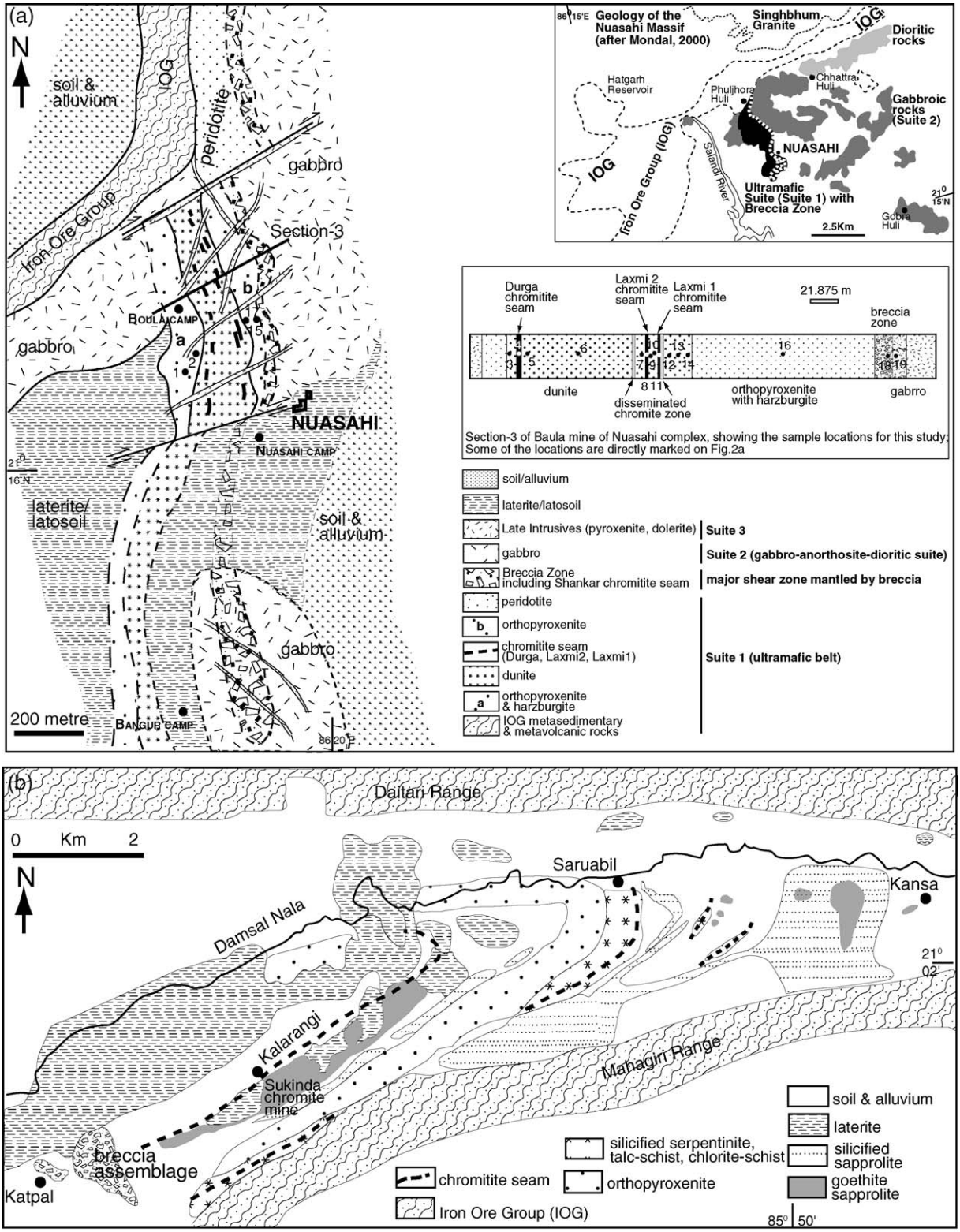

Fig. 2. Detailed map of the geology of the Nuasahi massif (a; after Mondal et al., 2001) and Sukinda massif (b; after Page et al., 1985). Inset map shows generalized geology of the Nuasahi area (after Mondal, 2000).

band with an average thickness of 3–4 m. The Laxmi-2 is 2–3 m thick, and Laxmi-1 is 1.6–2 m thick. In the footwall of Laxmi 2 and the hanging wall of Laxmi 1 there is a 2–4 m wide zone of disseminated chromite ores which parallel the main seam (Fig. 2a and Section 3). The chromitite seams are sheared, rotated and offset by a series of NE- and NNW-trending faults. Warping and minor folds in the ultramafic rocks are common in the southern sector of the Nuasahi massif.

In the Sukinda massif, chromitite seams occur as disconnected and irregular lenses or bands, and are folded and faulted along the 25 km long ultramafic belt. At least six dissected bands of massive chromitite seams are present (CB 1–6), ranging in length from 200 m to as much as 3000 m. Reserves of the chromitite ores are estimated to occur up to a depth of 250 m (Page et al., 1985). Two types of chromitite ore are present: (1) brown, friable ore at the deep weathered zone and (2) hard, lumpy ore. The seams vary in width from a few meters to about 20 m with almost vertical dips.

Mineral-graded layers are commonly present within the chromitite seams (Fig. 3). Several workers (e.g., Haldar, 1967; Mohanty and Saho, 1989) have reported size-graded layers within the seams and suggest that the ultramafic suite in the Nuasahi massif is right side up. The chromitite seams in both the Nuasahi and Sukinda massifs are commonly characterized by schlieren bands, clot-textured bands, net-textured massive bands, spotted bands, nodular and anti-nodular textured chromitite bands (Figs. 3 and 4). Both schlieren and spotted layers grade to massive chromitite bands and show rhythmic banding with thin olivine-rich layers. In the clot-textured

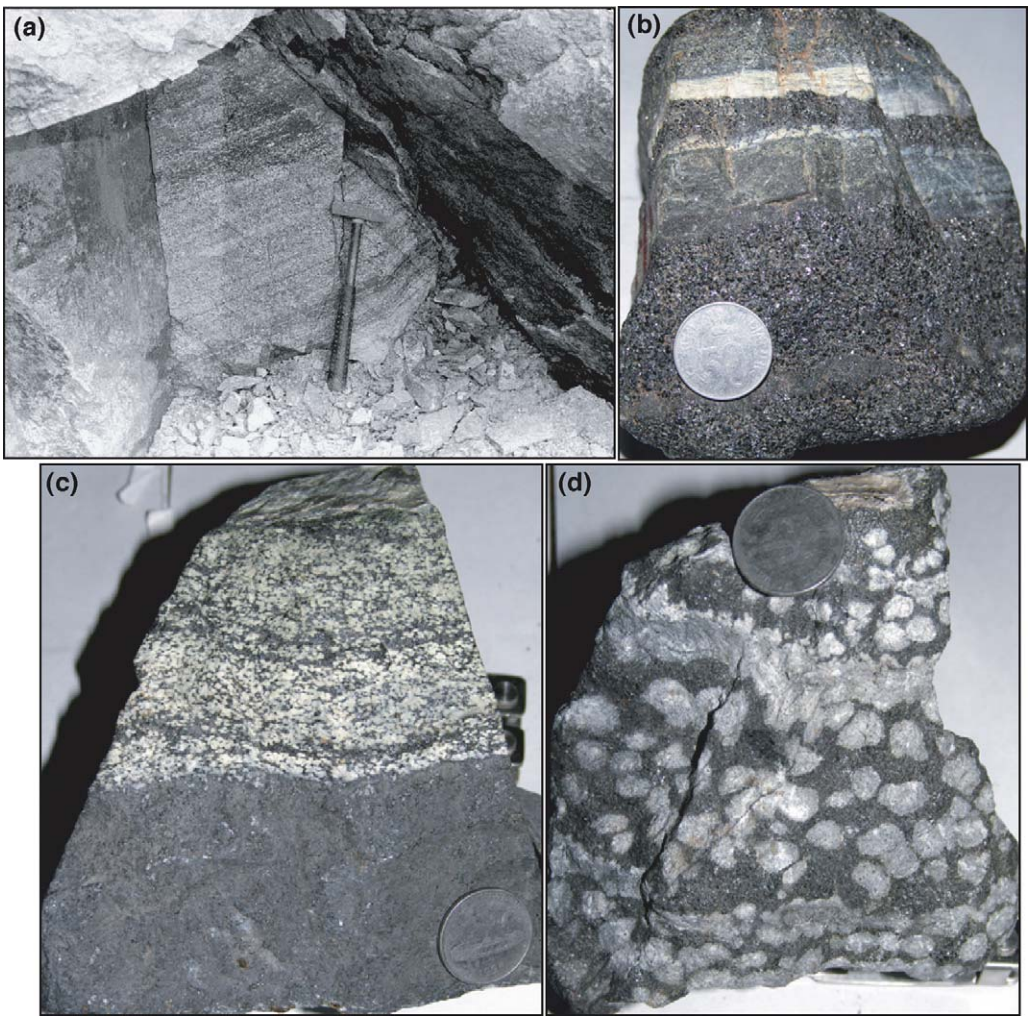

Fig. 3. Field photographs and hand specimen photographs. (a) Chromite-rich layers and olivine-rich layers forming rhythmic bands in chromitite seams; (b) banded chromitite within seams; (c) massive chromitite from seams, containing chromitite and olivine-rich schlieren bands; (d) chromitite interlayered with olivine-rich layers and containing rounded to elliptical olivine-rich clots (anti-nodular).

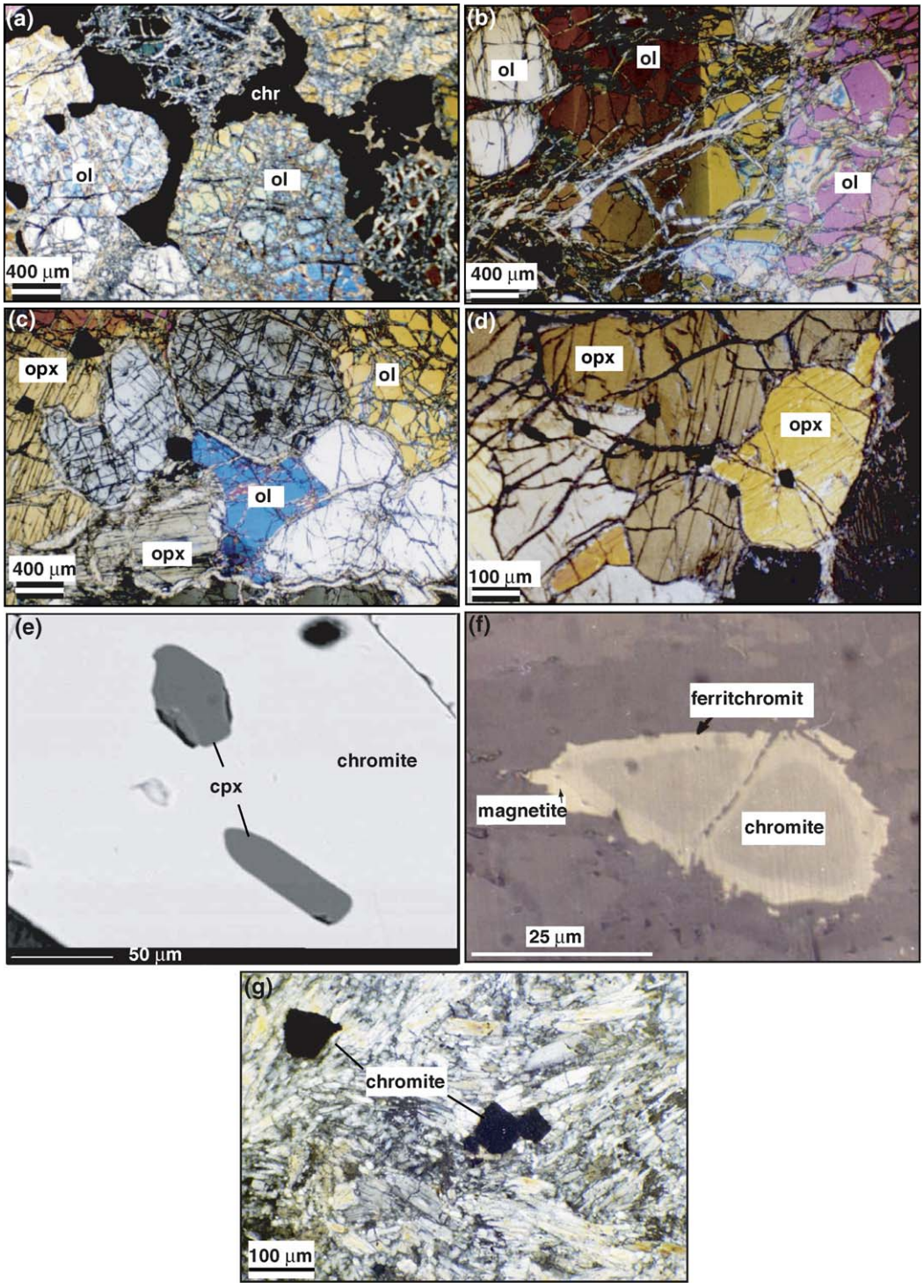

Fig. 4. Photomicrographs showing textures of different rocks. Dunite, orthopyroxenite (enstatitite) and harzburgite exhibit combination of protoclastic and intergranular textures formed by olivine (ol) and enstatite (opx). The vein materials are mostly serpentine, talc and chlorite along with magnetite/ferritchromit. (a) 'Chain- or net-texture' formed by intercumulus chromite (chr) in dunite. (b) lamellar twining in olivine in dunite; (c) harzburgite containing both included and intercumulus chromite. Olivine shows replacement relation with opx (left side); (d) euhedral chromite crystal poikilitically included within enstatite in orthopyroxenite; (e) clinopyroxene inclusions in chromite from massive chromitites; (f) chromite in serpentinized dunite. Ferritchromit rim is quite distinct at the grain boundary of chromite, where it is surrounded by magnetite rim; (g) subhedral to euhedral chromite crystals within IOG high-Mg metavolcanics rocks in the Nuasahi area. Silicate minerals are tremolite, actinolite, and chlorite.

chromitite band, the clots consist of fine-grained chromite that is embedded in a serpentinized matrix and occur within a relatively coarse-grained chromite rich matrix. In Nuasahi, chromitite seams show various gravity-controlled features such as slumping, overturned slump-folds, pseudo-current bedding and convolute structures (Mukherjee and Haldar, 1975). The nodular textured massive chromitite are characterized by the presence of sub-rounded to elliptical nodules (0.5–5 cm across) of fine-grained olivine-chromitite, which are embedded in the massive coarse-grained chromitite. In Sukinda, massive chromitite bands are often thinly laminated with alternate thin laminae (0.5–1.5 cm) of granular chromite and serpentinized olivine (Chakraborty and Chakraborty, 1984). The chromite crystals in the massive chromitite bands (>90–95 modal% chromite) are commonly fresh and contain interstitial phases such as serpentine, chlorite, talc, magnesite and sulfides. Relatively larger chromite grains are polygonal or sub-rounded, and commonly contain subhedral to euhedral silicate inclusions, mostly of clinopyroxene (Fig. 4e) along with minor orthopyroxene and olivine.

Disseminated chromite occurs in dunite, harzburgite and in orthopyroxenite (Fig. 4). Ferritchromit commonly occurs as a rim around original chromite crystals and itself is locally rimmed by magnetite in the more serpentinized part of the ultramafic rocks (Fig. 4f). Trails of minute grains of magnetite-ferritchromit are present in the talc- and chlorite-bearing serpentinized parts of the ultramafic unit (Fig. 4a–c). The IOG high-Mg metavolcanics rocks of komatiitic affinity from the Nuasahi area contain significant amounts of disseminated chromite grains (Fig. 4g) (Mondal, 2000; Mondal et al., 2003a). These are mostly subhedral to euhedral and show variable alteration to magnetite.

4.2. Ultramafic rocks

Medium- to coarse-grained olivine in dunite from the Nuasahi massif is mostly sub-rounded to rounded and in places intensely fractured (Fig. 4a). Serpentinite from the Sukinda massif shows remnants of original igneous textures, where serpentine-group minerals pseudomorphically replace olivine. Chromite is present as an accessory phase (<1–3%). Olivine grains are in mutual contact with each other and often show lamellar type of twinning with lenticular twin bands (Fig. 4b). In places olivine grains show undulose extinction. Olivine is partially altered to serpentine along fractures (Fig. 4a–c). In fault or shear zones dunite is extensively altered to an assemblage of talc-serpentine-chlorite ± magnesite ± quartz. Mondal and Baidya (1996) reported a hydrated chrome-carbonate phase, stichtite [$Mg_6Cr_2(OH)_{16}{\cdot}4H_2O{\cdot}CO_3$] in the serpentinized dunite in the Nuasahi massif. Stichtite mainly occurs as veins in serpentinites and, in places, as pseudomorphs of chromite crystals.

Harzburgite is medium to coarse-grained. It contains euhedral to subhedral accessory chromite grains (<1%; Fig. 4c). Chromites enclosed in enstatite and olivine crystals tend to be smaller than interstitial grains. Orthopyroxenite is medium to coarse-grained, and composed principally of enstatite (∼70%) and clino-enstatite (∼25–30%) (Fig. 4d). Large (∼5 cm) crystals of enstatite are common in orthopyroxenite, particularly in the western part of the Nuasahi massif. Accessory chromite (<1%) in this rock is mostly subhedral to euhedral and is commonly included in orthopyroxene crystals (Fig. 4d). Secondary minerals include talc, serpentine, chlorite, biotite, and magnetite/ferritchromit.

5. Analytical techniques and samples

Samples were collected from the chromitite seams as well as from the host lithologies in different mine sections. Samples from Section 3 in the Boula mine (northernmost sector of the ultramafic belt) and from the northern section of the Nuasahi mine (middle sector of the ultramafic belt) together with few chromitites from Bangur mine (southern sector of the ultramafic belt) were selected for detailed analytical work (Fig. 2a). The locations of these samples are shown in Fig. 2a. Samples from the Sukinda massif were collected from two sections of the Sukinda mine at Kalarangi (Fig. 2b). Both chromitites and the host rocks were collected from sections across the two major massive chromitite seams, known as CB 1 and CB 6. Samples of IOG high-Mg meta-igneous rocks were collected from the Nuasahi area. Chromite grains in massive chromitite from the G-chromitite horizon of the Stillwater Complex and the Railway Block of the Selukwe chromitite, Zimbabwe were also analyzed for comparative purposes.

Mineral compositions were determined by wavelength-dispersive X-ray analysis utilizing an acceleration voltage of 15 kV, a beam current of 20 nA, and a counting time of 20 s using the Cameca SX50 electron microprobe at Indiana University. The accuracy of quantitative analyses was monitored using reference materials of similar compositions. Sample reproducibility varied by less than 2% relative. Some of the mineral analyses were conducted using a JEOL-JXA 8600 electron microprobe at the Indian Institute of Technology (Roorkee) using an acceleration voltage of 15 kV, a beam current of 20 nA, and a counting time of 5 s. The SPI multi-standards were used for calibration.

Fe^{3+} in spinels was calculated according to the charge balance equation of Droop (1987).

6. Results of mineral analyses

6.1. Olivine and orthopyroxene

Representative analyses of olivine, pyroxene and chromite are listed in Table 2. The composition of olivine in dunite varies from Fo_{92} to Fo_{95} and that in harzburgite varies between Fo_{90} and Fo_{93}. The composition of olivine in spotted chromitites varies from Fo_{96} to Fo_{97}, whereas olivine in inclusions varies from Fo_{96} to Fo_{98}. The Fo contents of olivine show a positive relationship with NiO contents (Fig. 5a), but no systematic compositional variations with stratigraphic positions were found.

Table 2
Representative mineral compositions for olivine, orthopyroxene, clinopyroxene and chromite from the Nuasahi and Sukinda massifs

	Analysis Ref. 1:oli, NI-3	2:oli, D-12
SiO_2	41.27	41.29
MgO	49.44	50.64
NiO	0.26	0.36
FeO	8.94	7.50
Cr_2O_3	0.00	0.06
CaO	0.04	0.04
Total	99.95	99.88
Si	1.007	1.003
Mg	1.798	1.833
Ni	0.005	0.007
Fe	0.182	0.152
Cr	0.000	0.001
Ca	0.001	0.001
4 O	2.99	3.00
Mg#	90.81	92.34

	3:oli, D/1	4:oli, L1–24
SiO_2	42.12	42.24
MgO	53.06	53.35
NiO	0.50	0.45
FeO	4.18	3.96
Cr_2O_3	0.09	0.15
CaO	0.03	0.03
Total	99.97	100.18
Si	1.007	1.006
Mg	1.890	1.895
Ni	0.010	0.009
Fe	0.084	0.079
Cr	0.002	0.003
Ca	0.001	0.001
4 O	2.99	2.99
Mg#	95.74	96.00

Table 2 (*Continued*)

	5:opx, N-I/1	6:opx, L/34
SiO_2	57.88	56.62
TiO_2	0.04	0.13
Al_2O_3	0.06	0.16
FeO	5.04	6.44
Cr_2O_3	0.19	0.17
MnO	0.07	0.10
NiO	0.04	0.03
MgO	35.61	32.65
CaO	0.39	2.00
Na_2O	0.02	0.08
K_2O	0.01	0.01
Total	99.35	98.41
Si	1.996	1.994
Al	0.002	0.007
Fe	0.146	0.190
Mg	1.831	1.715
Mn	0.002	0.003
Ca	0.015	0.076
K	0.000	0.001
Na	0.001	0.006
Ti	0.001	0.003
Cr	0.005	0.005
Ni	0.001	0.001
6 O	4.0	4.0
%En	91.86	86.47
%Fs	7.41	9.73
%Wo	0.73	3.81
Mg#	92.54	89.89

	7:opx, SCM/49	8:opx, O-15a	9:cpx, O-15a
SiO_2	57.97	58.95	54.60
Al_2O_3	0.75	0.33	0.69
MgO	33.69	37.58	18.10
Na_2O	0.00	0.00	0.33
FeO	5.95	2.48	0.90
MnO	0.11	0.03	0.00
Cr_2O_3	0.56	0.97	1.61
K_2O	0.01	0.00	0.01
CaO	0.80	0.44	23.93
TiO_2	0.03	0.07	0.09
Fe_2O_3	0.00	0.00	0.20
Total	99.87	100.85	100.44
Si	1.997	1.983	1.969
Al	0.031	0.013	0.029
Mg	1.730	1.885	0.973
Na	0.000	0.000	0.023
Fe^{2+}	0.171	0.070	0.027
Mn	0.003	0.001	0.000
Cr	0.015	0.026	0.046
K	0.000	0.000	0.000
Ca	0.030	0.016	0.925
Ti	0.001	0.002	0.002
Fe^{3+}	0.000	0.000	0.005
6 O	3.98	4.00	4.00
%En	89.45	95.59	50.55
%Fs	9.00	3.60	1.40
%Wo	1.55	0.81	48.05
Mg#	90.86	96.37	97.30

Table 2 (*Continued*)

	10:chr, D-12	11:chr, NI-3	12:chr, SCM/49	13: chr, SCM/48	14:chr, h/49a	15:chr, SCM/35	16:chr, D-7	17:chr, O-91	18:chr, O-98	19:chr, D-9	20:chr, L2–28	21:chr, L3–30	22: chr, SCM-38	23: chr, SCM-39
SiO_2	0.01	0.04	0.02	0.03	0.06	0.02	0.04	0.005	0.01	0.02	1.29	0.02	0.05	0.09
Al_2O_3	14.53	10.09	9.97	1.26	0.70	14.15	9.81	7.119	9.38	9.87	9.91	10.49	11.70	10.79
MgO	11.27	9.92	2.77	2.63	0.03	10.85	13.92	14.077	14.48	14.11	13.17	14.17	13.89	13.52
NiO	0.09	0.08	0.02	0.38	0.07	0.11	0.17	0.134	0.16	0.15	0.19	0.10	0.10	0.08
FeO	17.24	18.27	29.34	27.21	30.95	17.70	12.27	11.712	11.21	11.90	12.83	12.08	12.83	12.92
Cr_2O_3	53.14	59.86	56.62	38.39	30.35	54.28	60.64	64.963	62.89	61.19	59.28	60.73	59.55	60.87
TiO_2	0.30	0.14	0.15	1.48	0.05	0.29	0.19	0.197	0.16	0.21	0.26	0.19	0.19	0.12
MnO	0.00	0.00	0.00	1.38	0.21	0.00	0.00	0.000	0.00	0.00	0.00	0.00	0.00	0.00
Fe_2O_3	3.15	0.71	0.49	25.80	36.19	2.00	2.58	1.616	0.86	1.77	1.86	2.01	1.91	0.95
Total	99.72	99.10	99.38	98.54	98.58	99.39	99.61	99.823	99.16	99.21	98.78	99.80	100.22	99.34
Si	0.002	0.010	0.005	0.010	0.019	0.005	0.009	0.001	0.003	0.005	0.335	0.0060	0.014	0.023
Al	4.418	3.170	3.289	0.441	0.252	4.331	2.992	2.189	2.864	3.015	3.030	3.1790	3.519	3.289
Mg	4.333	3.944	1.156	1.168	0.012	4.201	5.368	5.476	5.593	5.451	5.091	5.4320	5.286	5.212
Ni	0.019	0.017	0.004	0.091	0.016	0.023	0.036	0.028	0.034	0.031	0.039	0.0210	0.020	0.017
Fe^{2+}	3.720	4.074	6.873	6.787	7.932	3.847	2.656	2.556	2.429	2.578	2.782	2.5970	2.738	2.796
Cr	10.841	12.616	12.537	9.049	7.354	11.149	12.405	13.401	12.884	12.539	12.153	12.3430	12.018	12.448
Ti^{4+}	0.059	0.027	0.032	0.331	0.011	0.056	0.037	0.039	0.032	0.040	0.050	0.0370	0.036	0.024
Mn	0.000	0.000	0.000	0.348	0.054	0.000	0.000	0.000	0.000	0.000	0.000	0.0000	0.000	0.000
Fe^{3+}	0.612	0.142	0.103	5.792	8.346	0.391	0.501	0.317	0.168	0.345	0.362	0.3890	0.367	0.184
Total	24.0	24.0	24.0	24.0	24.0	24.0	24.00	24.01	24.007	24.0	23.84	24.0040	24.0	24.0
Cr#	0.71	0.80	0.79	0.95	0.97	0.72	0.81	0.86	0.82	0.81	0.80	0.80	0.77	0.79
Mg#	0.54	0.49	0.14	0.15	0.00	0.52	0.67	0.68	0.70	0.68	0.65	0.68	0.66	0.65
Fe^{3+}/R^{3+}	0.04	0.01	0.01	0.38	0.52	0.02	0.03	0.02	0.01	0.02	0.02	0.02	0.02	0.01

oli – olivine: 1, harzburgite; 2, dunite; 3, spotted chromitite from seam; 4, inclusion in chromite from massive chromitite layer of seam; pyx – pyroxene: 5, opx (Nuasahi) west; 6, opx (Nuasahi) east; 7, opx (Sukinda); 8, opx inclusion in chromite from massive chromitite layer of seam; 9, cpx inclusion in chromite from chromitite layer of seam; chr – chromite: 10, dunite; 11, harzburgite; 12, orthopyroxenite; 13, serpentinite; 14, IOG high-Mg metavolcanics from Nuasahi area; 15, net-textured chromitite from seam; 16, spotted chromitite from seam; 17–23, massive chromitite from seams.

Orthopyroxene in different units from Suite 1 from the Nuasahi massif and in orthopyroxenite from the Sukinda massif are magnesian-rich enstatite (Fig. 5b). In Nuasahi, the composition of orthopyroxnene in orthopyroxenite from the eastern part of Suite 1 (see Fig. 2a) is more evolved in character than in the western part (Fig. 5b and c). Orthopyroxene in harzburgite from Nuasahi and in orthopyroxenite from Sukinda are slightly enriched in Cr_2O_3 relative to orthopyroxenite from the Nuasahi massif (Fig. 5b). The composition of orthopyroxene in inclusions from massive chromitite layers is distinctly higher in *Mg*-number than is orthopyroxene from other assemblages (Fig. 5b). Both clinopyroxene and orthopyroxene in inclusions are characteristically enriched in Cr_2O_3 as well. In general, the compositions of orthopyroxene from different assemblages show a positive trend with a steep slope in an Al_2O_3 versus CaO plot (Fig. 5c).

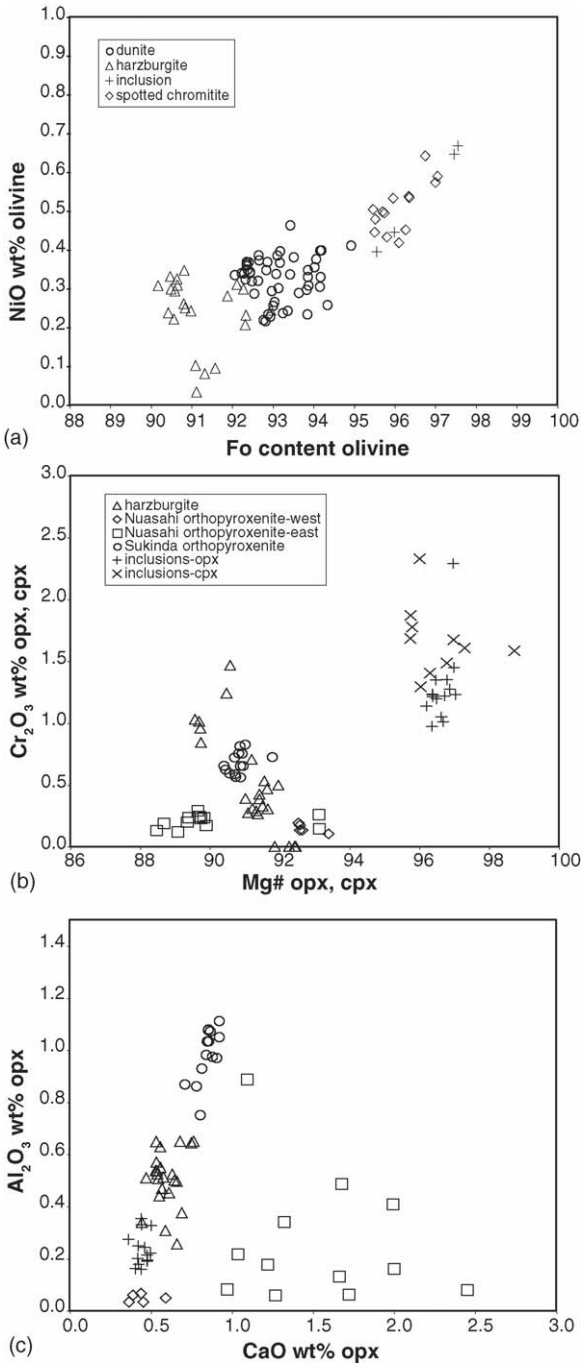

Fig. 5. Variation diagrams for composition of olivine and orthopyroxene from the Nuasahi and Sukinda massifs. (a) NiO–Fo content in olivine; (b) Cr_2O_3–Mg# in pyroxene; (c) CaO–Al_2O_3 variations in pyroxene. See text for details.

6.2. Chromite

Chromite in massive chromitite layers is characterized by high *Cr*-number (Cr/(Cr + Al), molar ratio) and high *Mg*-number ($Mg/(Fe^{2+} + Mg)$, molar ratio); for the Nuasahi massif the *Cr*-number is 0.78–0.87 and *Mg*-number is 0.66–0.82 and for the Sukinda massif the *Cr*-number is 0.75–0.81 and *Mg*-number is 0.62–0.73 (Fig. 6a). No systematic variations with stratigraphic positions were found. The composition of accessory chromite in dunite, orthopyroxenite and in net-textured chromitite layers from seams shows significant variations in both *Cr*-number and *Mg*-number (Fig. 6b). The composition varies on thin-section and hand-sample scales, but no systematic variations with stratigraphic positions are observed. Chromite in harzburgite shows a restricted composition in contrast with other accessory chromite (Fig. 6b). There is no systematic compositional variation found between poikilitically included chromite in silicate minerals and the chromites in interstitial spaces. The chromites in serpentinite from the Sukinda massif is characterized by low *Mg*-number and a strong variation in *Cr*-number (Fig. 6c). Chromites in serpentinite are also enriched in TiO_2 (Fig. 6g). In a Cr–Al–Fe^{3+} ternary diagram (Fig. 6d), the chromites show two distinct compositional trends: (1) accessory chromites have constant Cr/Fe^{3+} ratios and variable Cr/Al ratios and (2) chromites in serpentinites show variation in Fe^{3+} with a moderate range in Cr/Al ratios. The chromite compositions in high-Mg metavolcanics of the IOG (Fig. 4g) from Nuasahi area are Al depleted and Fe-rich (Fig. 6f).

The shaded fields on Fig. 6d–f show the compositional range of natural spinels from different geological environments as identified by Roeder (1994) and Barnes and Roeder (2001). Fields I–III are marked by Mondal et al. (2001) based on distribution of data points of chromite compositions of Roeder (1994). Field I represents spinels in primitive basaltic rocks, mantle peri-

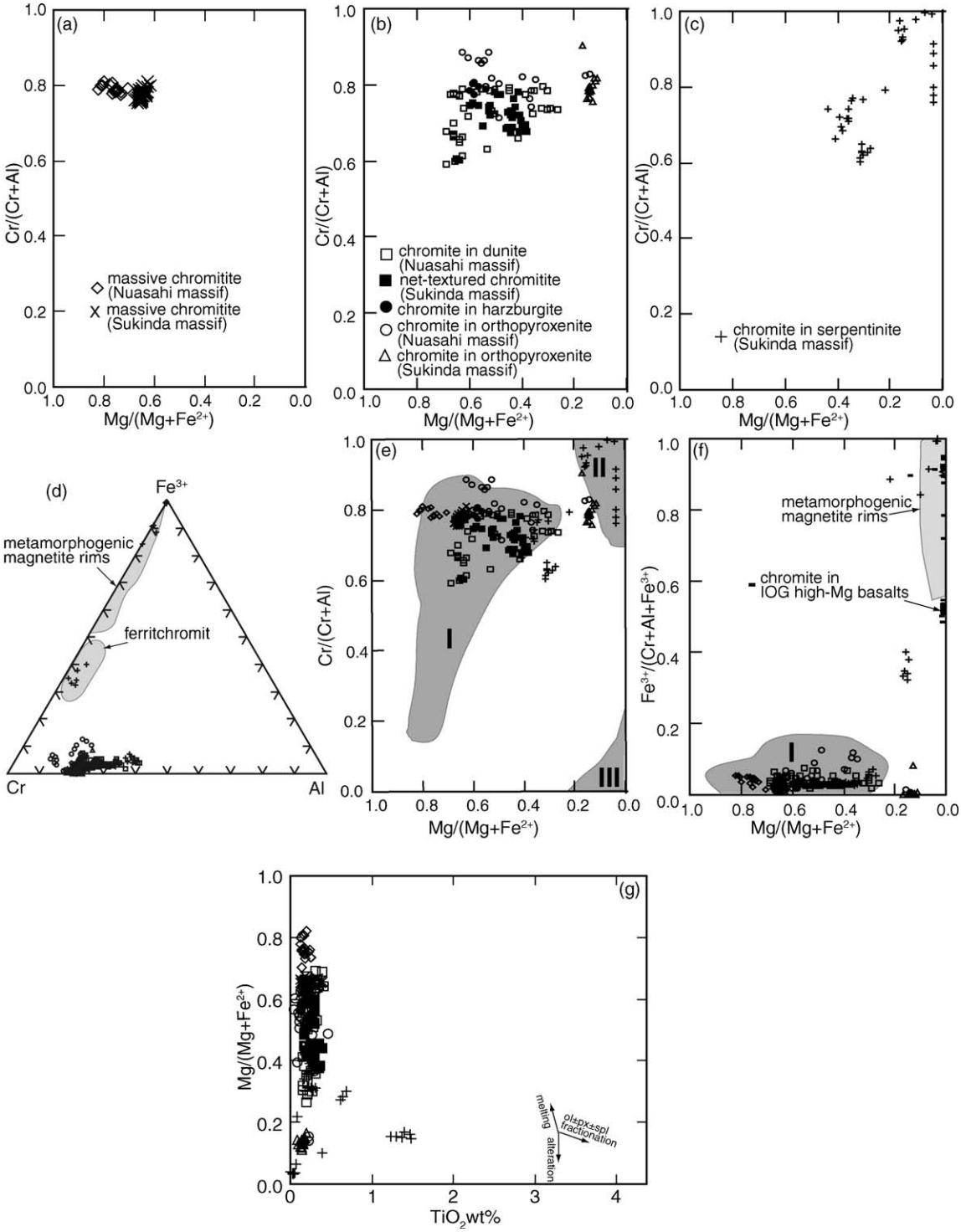

Fig. 6. Variation diagrams for composition of chromite from the Nuasahi and Sukinda massifs. (a) Cr#–Mg# variation seen in chromites from massive chromitite of seams; (b) Cr#–Mg# variation seen in accessory chromites from dunite, orthopyroxenite, harzburgite and net-textured chromitite; (c) Cr#–Mg# variation seen in chromites from serpentinite; (d) Cr–Al–Fe^{3+} variation seen in chromites of the Nuasahi and Sukinda massif (shaded fields are from Barnes and Roeder, 2001); (e) Cr#–Mg# variations of chromites of the present study (fields are based on data points of Roeder, 1994 and marked by Mondal et al., 2001); (f) trivalent cation ratios vs. Mg# variation from chromites of the present study (field I is marked by Mondal et al., 2001 based on data points of Roeder, 1994; other fields are from Barnes and Roeder, 2001); (g) Mg#–TiO_2 of chromites with respect to melting, alteration and fractionation trends as identified by Tesalina et al. (2003).

dotites and chromitites. Field II represents magnetite from metamorphic rocks and field III is magnetite from un-metamorphosed igneous rocks. Primary chromites in chromitites from the Nuasahi and Sukinda massifs are plotted within field I (Fig. 6a); the altered chromites from the present study are plotted in field II of metamorphic origin. The compositions of rims around altered chromite (see Fig. 4f) from serpentinized dunite or from serpentinite lies within the fields of metamorphic magnetite and ferritchromit (Fig. 6d–f). Many of the chromites (and the altered rims) in IOG high-Mg metavolcanic rocks lie within the field of metamorphic magnetite (Fig. 6f). The arrows in Fig. 6g show the approximate trends for chromite compositions related to peridotite partial melting, olivine ± pyroxene ± chromite fractionation and low-grade metamorphic alteration as identified by Tesalina et al. (2003). In massive chromitite as well as in dunite, harzburgite and orthopyroxenite, the *Mg*-number variations of chromite are distinct but do not correlate with their TiO_2 concentrations (Fig. 6g). The ferrianchromite in serpentinite shows a wide variation in *Mg*-number and TiO_2 concentration (Fig. 6g).

7. Discussion

7.1. Compositional variations of minerals, parental magma composition and implications for tectonic setting

The compositions of olivine in dunite, orthopyroxene in orthopyroxenite, and chromite in massive chromitite show only very limited variations. However, the compositions of those minerals are distinctly different and variable in other assemblages such as olivine from spotted chromitites and olivine inclusions in chromites, orthopyroxene inclusions in chromites, and chromite from dunite, harzburgite, and orthopyroxenite. In addition, although no systematic stratigraphic variations in the compositions of olivine, and chromite have been observed, compositional variations on hand-sample and thin-section scales are common. We suggest that such variations are related to subsolidus re-equilibration and secondary alteration processes. For example, the high *Mg*-number, coupled with elevated NiO and Cr_2O_3 contents, of olivine, orthopyroxene, and clinopyroxene inclusions in chromites from chromitites and of primocryst olivine in spotted chromitites, are strong lines of evidence for the re-equilibration of these minerals with associated chromite during cooling. Accessory chromite in dunite, harzburgite, and orthopyroxenite show large variations in both Cr/Al and Mg/Fe ratios with only small compositional changes in co-existing olivine and orthopyroxene. Observations that pertain to re-equilibration upon cooling and variation in the magnitude of mineral compositions related to abundance in the rock have been made by several researchers (e.g. Irvine, 1967; Jackson, 1969; Hamlyn and Keays, 1979; Eales and Reynolds, 1986). Although evidence for subsolidus re-equilibration is strong, positive correlations between olivine NiO content and *Mg*-number, and Al_2O_3 and CaO contents of orthopyroxene, suggest that primary trends produced during magmatic crystallization may, at least locally, be preserved during metamorphism and hydrothermal alteration. Our observations indicate that where olivine and chromite are modally abundant phases (i.e. dunites and chromitites), compositional changes due to exchange with interstitial liquids have been minimal. Small scale compositional variations related to metamorphism and alteration also appear to be minimal in dunites and chromitites. For this reason compositions of chromite from massive chromitites have been utilized to compute liquidus compositions which must be used in petrochemical calculations that pertain to parent magma characteristics.

We have calculated the Al_2O_3 content of the liquids in equilibrium with the chromitite by using the equation proposed by Maurel and Maurel (1982) for spinel-liquid equilibrium at 1 bar: $(Al_2O_3)_{spinel} = 0.035(Al_2O_3)^{2.42}$ (Al_2O_3 in wt.%). This formulation is constructed on the inference that Al_2O_3 in spinel is only a function of Al_2O_3 in the melt. The FeO/MgO ratio of the melt can be determined by using the formula proposed by Maurel and Maurel (1982): $\ln(FeO/MgO)_{spinel} = 0.47 - 1.07Y_{spinel}{}^{Al} + 0.64YFe_{spinel}{}^{3+} + \ln(FeO/MgO)_{liquid}$ with FeO and MgO in wt.%, $Y_{spinel}{}^{Al} = Al/(Cr + Al + Fe^{3+})$ and $Y_{spinel}{}^{Fe3+} = Fe^{3+}/(Cr + Al + Fe^{3+})$. The FeO/MgO ratio of the melt can also be calculated by using $K_D = 0.3$ for olivine (dunite)-liquid equilibrium and by using $K_D = 0.23$ for calcium-free pyroxene (orthopyroxenite)-liquid equilibrium (Roeder and Emslie, 1970). Calculated Al_2O_3 values and FeO/MgO ratios of the parental melts are given in Table 3. The results show little variation in parental melt compositions for the ultramafic rocks from Nuasahi and Sukinda massifs; the Al_2O_3 contents of the parent liquids for all the chromitites are similar. The values of FeO/MgO for the parent liquid obtained from chromitite compositions are similar to values obtained from dunite and orthopyroxenite (Table 3). However, the FeO/MgO ratios obtained for orthopyroxenite from the eastern part of the ultramafic suite in the Nuasahi massif are higher, indicating a slightly more fractionated parental magma. When compared with the compositions of primitive magma from different

Table 3
Calculation of Al_2O_3 content and FeO/MgO ratio of the melts in equilibrium with chromitite and other ultramafic rocks from the Nuasahi and Sukinda massifs

	Al_2O_3 liquid (wt.%)	FeO/MgO (wt.%) liquid
Archaean Nuasahi Massif		
Massive chromitite bands in seams	10.3–11.0	0.29–0.71
Orthopyroxenite (west)		0.54–0.62 ($K_D = 0.23$)opx
Orthopyroxenite (east)		0.86–1.00 ($K_D = 0.23$)opx
Dunite		0.32–0.51 ($K_D = 0.30$)oli
Archaean Sukinda Massif		
Massive chromitite band in seams	10.2–11.5	0.68–0.84
Orthopyroxenite		0.68–0.80 ($K_D = 0.23$)opx
IOG high-Mg basalts		
Nuasahi area[a]	7.9	0.52
Sukinda area[b]	10.7	0.94
Gorumahishani-Badampahar (Eastern) Belt[c]	8.8	0.91
Selukwe chromitite (Railway Block)	11.8–12.2	0.54–0.60
Stillwater G chromitite	12.3–12.6	1.48–1.58
Ophiolitic chromite deposits		
Oman chromitite[d]	11.4–16.4	0.62 ± 0.02
Layered Intrusions (parental magma)		
Bushveld (Average 'U' Type)[e]	11.5	0.74
Great Dyke[f]	11.1	0.61
Archaean low-Ti siliceous high-Mg basalts		
Barberton[g]	12.7–13.4	0.74
Pilbara[h]	10.1–11.7	0.58–0.75
Boninites[i]	10.6–14.4	0.7–1.4
MORB[i]	~15	1.2–1.6

[a] Mondal (2000).
[b] Basu et al. (1997).
[c] Sengupta et al. (1997).
[d] Augé (1987).
[e] Sharpe and Hulbert (1985).
[f] Wilson (1982).
[g] Jahn et al. (1982).
[h] Sun and Nesbitt (1978).
[i] Wilson (1989).

tectonic settings, our data fit best with the compositions of high temperature, low-Ti, siliceous high-Mg basalts ($Al_2O_3 = 10.05$–13.41 wt.%) in Archaean greenstone belts, or boninites ($Al_2O_3 = 10.6$–14.4 wt.% with low FeO/MgO ratios) in supra-subduction zone settings (Table 3).

In Fig. 7a the compositions of primitive chromite are plotted to compare with the compositional range of chromite from Achaean greenstone belts and from typical layered complexes of Archaean age. The comparison shows a similarity between the chromite compositions from the Nuasahi and Sukinda massifs and those from Archaean ultramafic complexes in greenstone belts (e.g. Selukwe, Zimbabwe with very high Cr/Fe_{total} and very low Ti content). Using *Cr*-number versus *Mg*-number and Cr–Al–Fe^{3+} relations, the liquidus chromites from the Nuasahi and Sukinda massifs plot within the boninitic field or the komatiitic field (Fig. 7b and c). It should be noted that the chromites in komatiites from greenstone belts (Fig. 7b) are commonly metamorphosed under green schist to amphibolite facies (Barnes, 2000). The fields on Fig. 7d and e have been identified by Kamenetsky et al. (2001) where the spinel compositions are distinguished based on tectonic setting and mode of occurrence using spinel TiO_2 versus Al_2O_3 and Fe^{2+}/Fe^{3+} versus Al_2O_3 diagrams. In these diagrams (Fig. 7d and e), the Nuasahi and Sukinda chromites from chromitites plot in the supra-subduction and back-arc field.

It is evident that the seam chromites from the Nuasahi and Sukinda massifs closely resemble chromites that crystallized from high-Mg, low-Al, supra-subdution

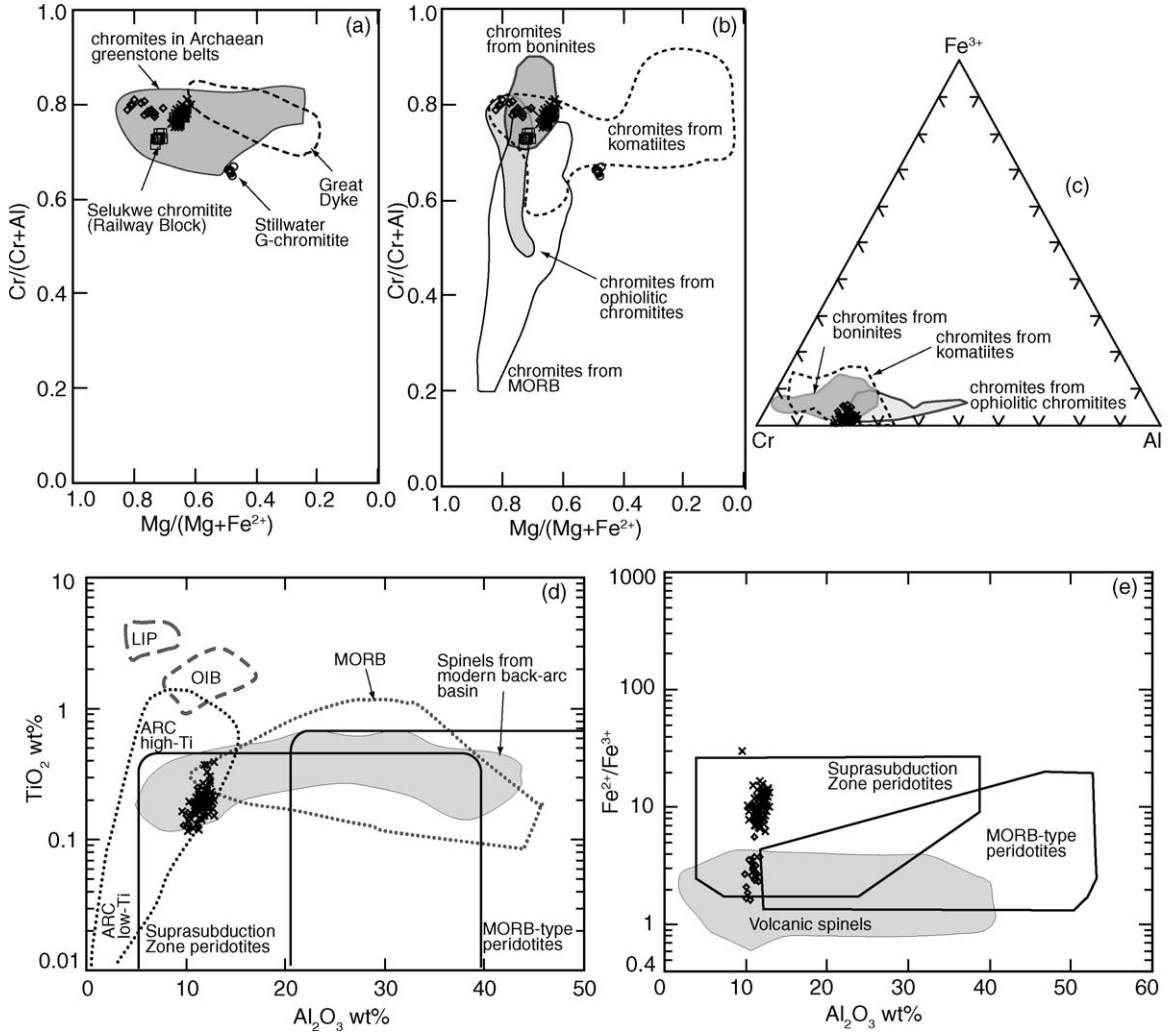

Fig. 7. Tectonic discrimination diagrams. (a) Cr#–Mg# variations in primitive chromites from within massive chromitites of the Nuasahi and Sukinda massifs and for chromites of other Archean occurrences. Fields are after Rollinson (1995b); (b) Cr#–Mg# variations in chromites compared with primitive magma (fields are after Barnes and Roeder, 2001); (c) trivalent cation plot of chromites from massive chromitite in comparison with chromites associated with boninites, ophiolites and komatiites (fields are after Barnes and Roeder, 2001); (d) TiO_2–Al_2O_3 variations seen in Cr-spinel with respect to modern-day tectonic-settings; (e) Fe^{2+}/Fe^{3+}–Al_2O_3 variations seen in Cr-spinel with respect to modern day tectonic settings and magmatic activities. Fields in (d) and (e) are from Kamenetsky et al. (2001).

zone related boninitic magma or a low Al-komatiitic magma in greenstone belts. Boninitic magmas are associated with subduction and back-arc rifting settings (Cameron et al., 1983) and are commonly proposed as being parental to the chromitites in Phanerozoic ophiolitic complexes, but rarely for ultramafic bodies and chromitites in Archaean greenstone belts. Boninitic magmas are characterized by high-SiO_2 (>55%), high-MgO (>9%), low TiO_2 (<0.3%) and high concentrations of compatible trace elements (Ni = 70–450 ppm, Cr = 200–1800 ppm) (Crawford et al., 1989). Such unique geochemical characteristics of boninites are thought to reflect incompatible trace element enrichment of a refractory (previously melted) source by a subduction-derived fluid or melt before remelting (i.e. second-stage melting), typically at low-pressure (<50 km) within supra-subduction zone settings (Sun and Nesbitt, 1978; Hicky and Frey, 1982). Siliceous, low-Ti, high-Mg basalts (komatiitic basalts) are common in Archaean greenstone belts, where these are closely associated with komatiites. Siliceous high Mg-basalts have similar major element compositions to boninites, and are thought to have been derived from komatiitic parents either by fractional crystallization and/or crustal contamination process (e.g. Barley, 1986; Cattell, 1987; Sun et al., 1989). Komatiites that are interlayered

Table 4
Comparison of compositions of high-Mg basaltic rocks from Nuasahi and Sukinda areas with other Archaean occurrence and Phanerozoic boninite from supra-subduction setting

Sample Ref. (age)	IOG (>3.1 Ga) Nuasahi H/49a[a]	IOG (>3.1 Ga) Sukinda GAWF/1/1[b]	IOG (>3.1 Ga) Eastern Belt: 39[c]	Pilbara (late Archaean) 331/337[d]	Cape Vogel (Phan.) boninite B6[e]
wt.%					
SiO_2	46.39	56.52	51.74	51.48	53.71
TiO_2	0.46	0.60	0.42	0.39	0.21
Al_2O_3	7.86	10.74	8.78	9.93	7.77
FeO_t	10.52	9.54	10.89	10.63	10.14
MnO	0.18	0.15	0.11	0.23	0.17
MgO	20.20	10.18	12.02	16.50	18.49
CaO	6.84	5.09	10.04	9.06	4.64
Na_2O	0.09	1.46	1.59	0.98	0.83
K_2O	0.34	0.39	0.04	0.34	0.19
P_2O_5		0.06	0.02	0.04	0.03
LOI	7.12	4.37	1.18	4.06	4.32
FeO/MgO	0.52	0.94	0.91	0.64	0.55
ppm					
Ba	91	40		135	30
Rb	6.7			8	
Sr	87			30	63
La	5.58	13.20	1.88	7.12	2.50
Ce	10.74	14.50	6.38	15.1	5.46
Nd	7.13	9.54		6.02	2.84
Sm	1.48	2.08	0.54	1.44	0.75
Eu	0.452	0.50	0.21	0.392	0.24
Tb	0.393	0.56	0.16		0.13
Dy	1.55	1.52		1.93	0.79
Yb	0.92	0.66	0.76	1.24	0.48
Lu	0.127	0.16	0.95		
Th	0.608				
U	0.69				
Zr	67			41	30
Hf	1.05		0.43		
Cs	0.220				
Ta	0.134				
As	81.5				
Sb	1.232				
Sc	15.89		13	28	24
Cr	4835	410	2130	2535	1930
Ni	1002	250	1590	471	540
Co	84.82		119	70	
Zn	104.1				
V	176.4			147	136

[a] Chromite-bearing IOG high-Mg metavolcanic (data source Mondal, 2000).
[b] Basu et al. (1997).
[c] Sengupta et al. (1997).
[d] Sun et al. (1989).
[e] Cameron et al. (1983).

with Archaean lavas which resemble modern ultramafic arc lavas (boninites) have been described by Kerrich et al. (1998). Boninites are also reported from several other Hadean and Archaean terraines (e.g. Polat et al., 2002; Smithies et al., 2004; Srivastava et al., 2004; Manikyamba et al., 2005). It should be noted that the IOG high-Mg basalts from the Singhbhum Craton are compositionally similar to boninites of subduction and back-arc rifting settings as documented in Table 4. Several workers (e.g. Allègre, 1982; Grove et al., 1999; Wilson et al., 2003) have suggested that some komatiites and komatiitic basalts within greenstone belts resulted from hydrous mantle melting at relatively low temperatures in supra-subduction setting. In addition, Parman et al. (2001) also

suggested that high-Mg basalts (komatiitic basalts) are the Archaean equivalents of boninites.

7.2. Origin of chromitites

Massive stratiform chromitite layers in large layered igneous intrusions can be traced for hundreds of km along strike. Although exposure does not permit the chromitite layers in the Sukinda and Nuasahi massifs to be traced for such distances, their geometries and stratigraphic position in ultramafic sequences are similar to those of chromitites in layered intrusions. Several mechanisms to generate the crystallization of chromite in greater than cotectic proportions have been proposed, and include: (1) silica addition (Irvine, 1975), (2) magma mixing (Irvine, 1977), (3) increase in oxygen fugacity during crystallization (Ulmer, 1969), (4) increase in total pressure (Lipin, 1993). Crustal contamination has been proposed by Rollinson (1997) to account for Archaean chromitites those are hosted in dunite and spatially associated with orthopyroxenite, and formed from komatiitic magma. He proposed that the assimilation of banded iron formation by a komatiitic melt would trigger orthopyroxene crystallization through the addition of silica, which in turn would raise the oxygen activity of the melt. Murck and Campbell (1986) showed that chromite stability is extremely sensitive to oxidation state of the magma and that a change in oxidation state of the magma may lead to chromite precipitation. However, a large change in magma oxidation state should also promote a change in *Mg*-numbers of olivine, and chromite in footwall and hanging wall rocks of the chromitite layers, which is absent in the present case. Moreover, trivalent cation plots for chromites in the Nuasahi and Sukinda chromitites indicate a reduced character for these chromitites, similar to that of reduced chromites commonly associated with Al-depleted komatiites or ophiolites (Barnes and Roeder, 2001). Finally, crustal contamination of komatiitic magma should be reflected in the isotopic composition of crystallized chromite. Our O isotopic studies show that the chromites in chromitite from the Nuasahi massif and other Archaean chromites in the greenstone belts (e.g. Selukwe chromitites of Zimbabwe Craton) are characterized by mantle-like $\delta^{18}O$ values rather than elevated values that are expected as a result of assimilation of high ^{18}O metasedimentary material (e.g. Mondal et al., 2003b). Therefore, crustal contamination may not be a viable process for chromitite genesis in the Sukinda and Nuasahi massifs.

Murck and Campbell (1986) have shown that Cr solubility is strongly temperature dependent at constant fO_2 whereas, the solubility increases at reducing condition and the effect is greater at higher temperature. They have showed that simple mixing of hot and cool chromite-saturated melts will force chromite supersaturation in the mixture, independent of other compositional effects. However, magmas of different temperatures should also be characterized by different compositions; evidence for such mixing is absent in the Nuasahi and Sukinda massifs. Irvine (1977) proposed that chromitites may form by injection and mixing of a primitive magma into a chamber of more fractionated magma. However, the very narrow range of olivine Fo in dunite from Nuasahi strongly suggests that if different magmas did mix they were of similar composition. Knowledge of the solubility of chromite as a function of T, P, fO_2, and melt composition would be required to rigorously evaluate the mixing model for chromite genesis.

In addition to magma mixing, fluids may play an important role in the formation of chromitites at relatively low pressure. For example, the experiments of Sisson and Grove (1993) and Gaetani et al. (1994) show that H_2O destabilizes silicate minerals relative to hydrous silicate liquid, but does not destabilize oxide phases to a comparable extent. Sisson and Grove (1993) observed that the effect of H_2O-saturation at 2 kb is to lower the crystallization temperatures of silicates by over 150 °C relative to their crystallization temperature at 1 bar and anhydrous conditions. Experiments by Ford et al. (1972) on lunar high-alumina basalt also show that the addition of H_2O stabilizes spinel on the liquidus at low pressure (2 kb), whereas under anhydrous conditions spinel appears on the liquidus at over 10 kb. Therefore, high water concentrations in a primitive melt would be expected to lower the liquidus temperature of silicates and cause chromite to be the first phase to crystallize (e.g. Nicholson and Mathez, 1991; Bannister et al., 1998). It is possible that a combination of magma mixing involving a boninitic or high-Mg siliceous basaltic magma, coupled with relatively high water contents of the mixed magma in a supra-subduction zone setting may be responsible for the chromitites in the Nuasahi and Sukinda massifs (Fig. 8).

7.3. Broader implications

The Singhbhum Craton in the Singhbhum-North Orissa Province records a long and nearly continuous tectonic evolution from early Archaean to middle Proterozoic ages. Our results indicate that the chromitites of the Nuasahi and Sukinda massifs in the Singhbhum Craton were crystallized from a mantle-derived boninitic or siliceous high-Mg basaltic magma that intruded into the volcano-sedimentary greenstone belts, but evidence

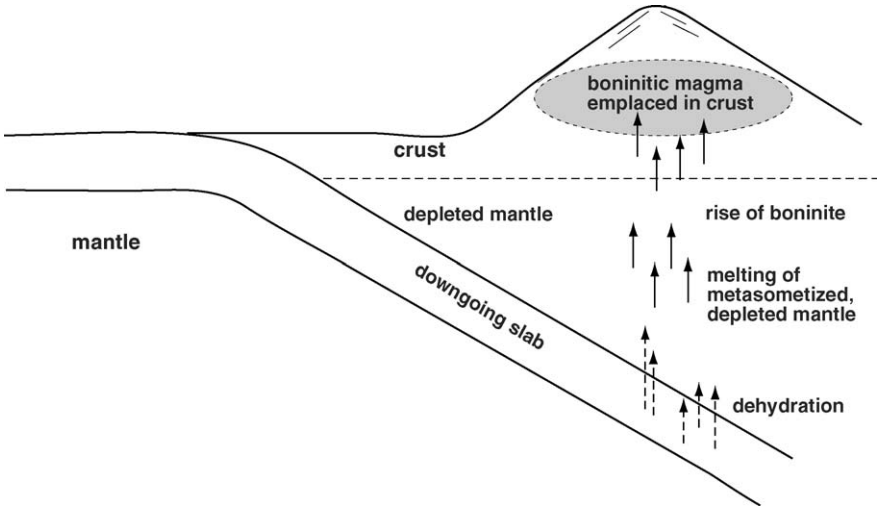

Fig. 8. Schematic representation of possible sub-arc setting over a subduction zone for the formation of ultramafic rocks of the Nuasahi and Sukinda massifs. Melting of metasomatized depleted mantle accompanied by fluids derived from the subducting slab could account for the geochemical characteristics of the chromitites in the Nuasahi and Sukinda massifs.

for crustal contamination of the magmas is minimal. The primitive mineral compositions of chromite, olivine, and orthopyroxene in monomineralic rocks suggest that their parental magmas were formed by high degree of mantle melting that characterized the Archaean magmatism. We propose that parental boninitic magmas were produced due to second-stage melting of a depleted upper mantle in presence of fluids derived from the subducting slab in a supra-subduction zone setting (Fig. 8).

8. Conclusions

(1) Chromite compositions from massive chromitites in the Nuasahi and Sukinda massifs show little variation and largely preserve primitive liquidus compositions, whereas accessory chromites show evidence of extended re-equilibration during low-grade metamorphism. The compositions of chromites from IOG high-Mg metavolcanics were extensively modified due to low-grade metamorphism and are similar to that of altered chromites of the intrusive ultramafic rocks in Nuasahi and Sukinda massifs.
(2) Liquidus chromite composition plots and calculated parental magma compositions suggest that the chromitites and associated ultramafic rocks in the Nuasahi and Sukinda massifs crystallized from a low Ti-high-Mg siliceous magma or boninite. Our data also suggest that the parental boninitic magma may be genetically linked with the spatially associated chromite-bearing IOG high-Mg basalts in the area.
(3) The combination of magma mixing involving a boninitic magma and relatively high water contents in the magmas derived from upper mantle in a supra-subduction zone setting can best explain the origin of the chromitites in the Nuasahi and Sukinda massifs.

Acknowledgements

The TISCO Ltd., FACOR Ltd., OMC and IMFA Corp. provided logistic support during fieldwork. M.K. Pujari, K.N.G. Rao, Kiran C. Goswami, D.P. Mishra and S. Nayek are acknowledged for their help during fieldwork in the Nuasahi and Sukinda areas. This research has been financially supported by the DST as a 'BOYSCAST' Fellowship to SKM in Indiana University and as 'Leave on Deputation' from Jadavpur University. Some of the EPMA work was conducted with financial help from the CSIR, New Delhi. Lou Bucklin guided sample preparation at Indiana University. Clive Stowe generously donated samples of Selukwe chromitite from his collections and is thankfully acknowledged. Peter Roeder and Ed Mathez are gratefully acknowledged for their critical comments and review of the earlier version of the manuscript. This paper is highly benefited from the critical reviews by the two journal reviewers. We are thankful to Kenneth Eriksson for his editorial handling of this manuscript. SKM is grateful to the late Eugene F. Stumpfl for his support and continuous encouragement through several communications on diverse aspects of research and collaboration on the Nuasahi massif since 1995.

References

Acharyya, S.K., 1993. Greenstones from Singhbhum Craton, their Archaean character, oceanic crustal affinity and tectonics. Proc. Natl. Acad. Sci. India 63 (A), 211–222.

Allègre, C.J., 1982. Genesis of Archaean komatiites in a wet ultramafic subducted plate. In: Arndt, N.T., Nisbet, E.G. (Eds.), Komatiites. George Allen and Unwin, pp. 495–500.

Augé, T., 1987. Chromite deposits in the northern Oman ophiolite: mineralogical constraints. Miner. Dep. 22, 1–10.

Augé, T., Cocherie, A., Genna, A., Armstrong, R., Guerrot, C., Mukherjee, M.M., Patra, R.N., 2003. Age of the Baula PGE mineralization (Orissa India) and its implications concerning the Singhbhum Archaean Nucleus. Precambrian Res. 121, 85–101.

Banerjee, P.K., 1972. Geology and geochemistry of the Sukinda ultramafic field, Cuttack district, Orissa. Memoir Geol. Surv. India 103, 171.

Barley, M.E., 1986. Incompatible element enrichment in Archaean basalts: a consequence of contamination by older sialic crust rather than mantle heterogeneity. Geology 14, 1–15.

Barnes, S.J., 2000. Chromite in Komatiites. II. Modification during greenschist to mid-amphibolite facies metamorphism. J. Petrol. 41, 387–409.

Barnes, S.J., Roeder, P.L., 2001. The range of spinel compositions in terrestrial mafic and ultramafic rocks. J. Petrol. 42, 2279–2302.

Basu, A., Maitra, M., Roy, P.K., 1997. Petrology of mafic-ultramafic complex of Sukinda valley, Orissa. Indian Miner. 50, 271–290.

Bannister, V., Roeder, P., Poustovetov, A., 1998. Chromite in the Paricutin lava flows (1943–1952). J. Volcanol. Geoth. Res. 87, 151–171.

Chakraborty, K.L., Chakraborty, T.L., 1984. Geological features and origin of the chromite deposits of Sukinda valley, Orissa, India. Miner. Dep. 19, 256–265.

Cameron, W.E., McCulloch, M.T., Walker, D.A., 1983. Boninite petrogenesis: chemical and Nd–Sr isotopic constraints. Earth Planet. Sci. Lett. 65, 75–89.

Cattell, A., 1987. Enriched Komatiitic basalts from Newton Township, Ontario: their genesis by crustal contamination of depleted Komatiitic magma. Geol. Mag. 124, 303–309.

Crawford, A.J., Falloon, T.J., Green, D.H., 1989. Classification, petrogenesis and tectonic setting of boninites. In: Crawford, A.J. (Ed.), Boninites. Unwin Hyman, London, pp. 2–44.

Dick, H.J.B., Bullen, T., 1984. Chromian spinel as a petrogenetic indicator in abyssal and alpine-type peridotites and spatially associated lavas. Contrib. Mineral. Petrol. 86, 54–76.

Droop, G.T.R., 1987. A general equation for estimating Fe^{+3} concentrations in ferromagnesian silicates and oxides from microprobe analysis, using stoichiometric criteria. Miner. Mag. 51, 431–435.

Eales, H.V., Reynolds, I.M., 1986. Cryptic variations within chromitites of the Upper Critical Zone, northwestern Bushveld complex. Econ. Geol. 81, 1056–1066.

Evans, B.W., Frost, B.R., 1975. Chrome-spinel in progressive metamorphism-a preliminary analysis. Geochim. Cosmochim. Acta 39, 959–972.

Ford, C.E., Bigger, G.M., Humphries, D.J., Wilson, G., Dixon, D., O'Hara, M.J., 1972. Role of water in the evolution of the lunar crust; an experimental study of sample 14310; an indication of lunar calc-alkaline volcanism. Proc. Third Lunar Sci. Conf. 1, 207–229.

Gaetani, G.A., Grove, T.L., Bryan, W.B., 1994. Experimental phase relations of basaltic andesite from hole 839B under hydrous and anhydrous conditions. In: Hawkins, J., Parson, L., Allan, J. (Eds.), Proceedings of the Ocean Drilling Program: Scientific Results, vol. 135, pp. 557–563.

Grove, T.L., Parman, S.W., Dann, J.C., 1999. Conditions of magma generation for Archaean komatiites from the Barberton Mountainland, South Africa. In: Fei, Y., Bertka, C.M., Mysen, B.O. (Eds.), Mantle Petrology; Field Observations and High-Pressure Experimentation; a tribute to Francis R. (Joe) Boyd, vol. 6. Geochemical Soc., Houston, pp. 155–167.

Ghosh, A.M.N., Prasada Rao, G.H.S.V., 1952. Some observations on the chromite occurrences of Nuasahi, Keonjhar district, Orissa. Rec. Geol. Surv. India 82, 281–299.

Haldar, D., 1967. Some observations on the chromiferous ultramafic and the associated rocks around Nuasahi, Keonjhar district, Orissa. Indian Miner. 21, 196–204.

Hamlyn, P.R., Keays, R.R., 1979. Origin of chromite compositional variation in the Panton Sill, Western Australia. Contrib. Mineral. Petrol. 69, 75–82.

Hicky, R.L., Frey, F.A., 1982. Geochemical characteristics of boninite series volcanics: implications for their source. Geochim. Cosmochim. Acta 46, 2099–2115.

Irvine, T.N., 1967. Chromian spinel as a petrogenetic indicator. Part II. Petrological applications. Can. J. Earth Sci. 4, 71–103.

Irvine, T.N., 1975. Crystallization sequences in the Muskox intrusion and other layered intrusions-II. Origin of chromitite layers and similar deposits of other magmatic ores. Geochim. Cosmochim. Acta 39, 991–1020.

Irvine, T.N., 1977. Origin of chromitite layers in the Muscox intrusion and other stratiform intrusions: a new interpretation. Geology 5, 273–277.

Jackson, E.D., 1969. Chemical variation in coexisting chromite and olivine in chromitite zones of the Stillwater complex. Econ. Geol. Monogr. 4, 41–71.

Jahn, B.-M., Gruau, G., Glikson, A.Y., 1982. Komatiites of the Onverwacht Group, South Africa: REE geochemistry, Sm/Nd age and mantle evolution. Contrib. Mineral. Petrol. 80, 25–40.

Kamenetsky, V.S., Crawford, A.J., Meffre, S., 2001. Factors controlling chemistry of magmatic spinel: an empirical study of associated olivine, Cr-spinel and melt inclusions from primitive rocks. J. Petrol. 42, 655–671.

Kerrich, R., Wyman, D., Fan, J., Bleeker, W., 1998. Boninite series; low Ti-tholeiite associations from the 2.7 Ga Abitibi greenstone belt. Earth Planet. Sci. Lett. 164, 303–316.

Leelananadam, C., Burke, K., Ashwal, L.D., Webb, S.J., 2006. Proterozoic mountain building in Peininsular India: an analysis based primarily on alkaline rock distribution. Geol. Mag. 143, 1–18.

Lipin, B.R., 1993. Pressure increases in the formation of chromite seams and the development of the ultramafic series in the Stillwater complex, Montana. J. Petrol. 34, 955–976.

Majumder, R., Bose, P.K., Sarkar, S., 2000. A commentary on the tectono-sedimentary record of the pre-2.0 Ga continental growth of India vis-à-vis a possible pre-Gondwana Afro-Indian supercontinent. J. African Earth Sci. 30, 201–217.

Manikyamba, C., Naqvi, S.M., Rao, D.V.S., Mohan, M.R., Khanna, T.C., Rao, T.G., Reddy, G.L.N., 2005. Boninites from the Neoarchaean Gadwal Greenstone belt, eastern Dharwar Craton, India: implications for Archaean subduction processes. Earth Planet. Sci. Lett. 230, 65–83.

Maurel, C., Maurel, P., 1982. Etude expérimentale de la solubilité du chrome dans les bains silicatés basiques et sa distribution entre liquide et minéraux coexistants: conditions d'existence du spinelle chromifére. Bulletin Minéralogie 105, 197–202.

Mishra, S., Deomuarari, M.P., Wiedenbeck, M., Goswami, J.N., Ray, S., Saha, A.K., 1999. $^{207}Pb/^{206}Pb$ zircon ages and the evolution of the Singhbhum Craton, eastern India: an ion microprobe study. Precambrian Res. 93, 139–151.

Mohanty, J.K., Saho, R.K., 1989. Chemistry of chromites from Boula-Nausahi Igneous Complex, Keonjhar dist., Orissa and its petrogenetic significance. J. Geol. Soc. India 33, 321–331.

Mondal, S.K., 2000. Study of chromite, sulfide, and noble metal mineralization in the Precambrian Nuasahi ultramafic-mafic complex, Keonjhar district, Orissa, India. Unpublished PhD Thesis. Jadavpur University, Calcutta, India, p. 193.

Mondal, S.K., Baidya, T.K., 1996. Stichtite [$Mg_6Cr_2(OH)_{16}CO_3{\cdot}4H_2O$] in Nuasahi ultramafites, Orissa, India—its transformation at elevated temperatures. Mineral. Mag. 60, 836–840.

Mondal, S.K., Baidya, T.K., 1997. Platinum-group mineral from the Nuasahi ultramafic-mafic complex, Orissa, India. Mineral. Mag. 61, 902–906.

Mondal, S.K., Baidya, T.K., Rao, K.N.G., Glascock, M.D., 2001. PGE and Ag mineralization in a breccia zone of the Precambrian Nuasahi Ultramafic-mafic Complex, Orissa, India. Can. Mineral. 39, 979–996.

Mondal, S.K., Glascock, M.D., Ripley, E.M., 2002. Characteristics of Cr-spinel and whole rock geochemistry of the Nuasahi Igneous Complex, Orissa, India. In: Proceedings of the Ninth International Pt-Symposium, Billings, Montana, Abstract with program, pp. 317–320.

Mondal, S.K., Ripley, E.M., Li, C., Sarkar, A., 2003a. Chemical composition and significance of Cr-spinel in Archaean greenstone belt ultramafic-mafic intrusive and extrusive rocks of the Singhbhum Craton, Eastern India. GAC-MAC-SEG joint meeting at Vancouver, Abstract with program, Abstract No. 616.

Mondal, S.K., Ripley, E.M., Li, C., Ahmed, A.H., Arai, S., Liipo, J., Stowe, C., 2003b. Oxygen isotopic compositions of Cr-spinels from Archaean to Phanerozoic chromite deposits. Goldschmidt conference abstract published in Geochim. Cosmochim. Acta, 18S, A301.

Mukherjee, S., Haldar, D., 1975. Sedimentary structures displayed by the ultramafic rocks of Nuasahi, Keonjhar district, Orissa, India. Miner. Dep. 10, 109–119.

Mukhopadhyay, D., 1988. Precambrian of the Eastern Indian shield-perspective of the problems. In: Mukhopadhyay, D. (Ed.), Precambrian of the Eastern Indian Shield. Memoir. Geol. Soc. India 8, 1–12.

Mukhopadhyay, D., 2001. The Archaean nucleus of Singhbhum: the present state of knowledge. Gondwana Res. 4, 307–318.

Mukhopadhyay, D., Dutta, D.R., 1983. Structures in the Roro ultramafics and their country rocks, Singhbhum district, Bihar. In: Sinha-Roy, S. (Ed.), Structure and Tectonics of Precambrian Rocks of India. Recent Researches in Geology, vol. 10. Hindustan Publishing Corpn., Delhi, pp. 98–109.

Murck, B.N., Campbell, I.H., 1986. The effects of temperature, oxygen fugacity and composition on the behavior of chromium in basic and ultramafic melts. Geochim. Cosmochim. Acta 50, 1871–1887.

Nicholson, D.M., Mathez, E.A., 1991. Petrogenesis of the Merensky Reef in the Rustenburg section of the Bushveld Complex. Contrib. Mineral. Petrol. 107, 293–309.

Page, N.J., Banerjii, P.K., Haffty, J., 1985. Characterization of the Sukinda and Nausahi ultramafic complex, Orissa, India by platinum-group element geochemistry. Precambrian Res. 30, 27–41.

Pal, T., Mitra, S., 2004. P–T–fo_2 controls on a partly inverse chromite-bearing ultramafic intrusive: an evaluation from the Sukinda Massif, India. J. Asian Earth Sci. 22, 483–493.

Parman, S.W., Grove, T.L., Dann, J.C., 2001. The production of Barberton komatiites in an Archaean subduction zone. Geophys. Res. Lett. 28, 2513–2516.

Polat, A., Hofmann, A.W., Rosing, M.T., 2002. Boninite-like volcanic rocks in the 3.7–3.8 Ga Isua greenstone belt, West Greenland: geochemical evidence for intra-oceanic subduction zone processes in the early earth. Chem. Geol. 184, 231–254.

Radhakrishna, B.P., Naqvi, S.M., 1986. Precambrian continental crust of India and its evolution. J. Geol. 94, 145–166.

Roeder, P.L., 1994. Chromite: from the fiery rain of chondrules to the Kilauea Iki lava lake. Can. Mineral. 32, 729–746.

Roeder, P.L., Emslie, R.F., 1970. Olivine-liquid equilibria. Contrib. Mineral. Petrol. 29, 275–289.

Rollinson, H., 1995a. Composition and tectonic settings of chromite deposits through time. Econ. Geol. 90, 2091–2092.

Rollinson, H., 1995b. The relationship between chromite chemistry and the tectonic setting of Archaean ultramafic rocks. In: Blenkinsop, T.G., Tromps, P. (Eds.), Sub-Saharan Econ. Geol. Amsterdam. Balkema, pp. 7–23.

Rollinson, H., 1997. The Archaean komatiite-related Inyala chromitite, Southern Zimbabwe. Econ. Geol. 92, 98–107.

Rollinson, H., Appel, P.W.U., Frei, R., 2002. A metamorphosed, early Archaean chromitite from west Greenland: implications for the genesis of Archaean anorthosite chromitites. J. Petrol. 43, 2143–2170.

Roy, A., Sarkar, A., Jeyakumar, S., Aggrawal, S.K., Ebihara, M., 2002. Sm–Nd age and mantle source characteristics of the Dhanjori volcanic rocks, Eastern India. Geochem. J. 36, 503–518.

Roy, A., Sarkar, A., Jeyakumar, S., Aggrawal, S.K., Ebihara, M., Satoh, H., 2005. Late Archaean mantle metasomatism below eastern Indian craton: evidence from trace elements, REE geochemistry and Sr–Nd–O isotope systematics of ultramafic dykes. Proc. Indian Acad. Sci. (Earth Planet. Sci.) 113, 649–665.

Saha, A.K., 1994. Crustal evolution of Singhbhum North Orissa, Eastern India. Geol. Soc. India Memoir 27, 341.

Saha, A.K., Ray, S.L., Sarkar, S.N., 1988. Early history of the Earth: evidence from the eastern Indian Shield. In: Mukhopadhyay, D. (Ed.), Precambrian of the Eastern Indian Shield. Memoir. Geol. Soc. India 8, 13–37.

Sarkar, N.K., Mallik, A.K., Panigrahi, D., Ghosh, S.N., 2001. A note on the occurrence of breccia zone in the Katpal chromite lode, Dhenkanal district, Orissa. Indian Miner. 55 (3–4), 247–250.

Sengupta, S., Acharya, S.K., De Smeth, J.B., 1997. Geochemistry of Archaean volcanic rocks from Iron Ore supergroup, Singhbhum, eastern India. Proc. Indian Acad. Sci. (Earth Planet. Sci.) 106, 327–342.

Sharpe, M.R., Hulbert, L.J., 1985. Ultramfic Sills beneath the Eastern Bushveld complex: mobilized suspensions of early lower zone cumulates in a parental magma with boninitic affinities. Econ. Geol. 80, 849–871.

Sharma, M., Basu, A.R., Ray, S.L., 1994. Sm–Nd isotopic and geochemical study of the Archaean tonalite-amphibolite association from the eastern Indian craton. Contrib. Mineral. Petrol. 117, 45–55.

Sisson, T.W., Grove, T.L., 1993. Experimental investigations of the role of H_2O in calc-alkaline differentiation and subduction zone magmatism. Contrib. Mineral. Petrol. 113, 143–166.

Smithies, R.H., Champion, D.C., Sun, S.-S., 2004. The case for Archaean boninites. Contrib. Mineral. Petrol. 147, 705–721.

Srivastava, R.K., Singh, R.K., Verma, S.P., 2004. Neoarchaean mafic volcanic rocks from the southern Bastar greenstone belt, Central India: petrological and tectonic significance. Precambrian Res. 131, 305–322.

Srinivasachari, K., 1974. Stratiform chromite deposits of Sukinda-Nuasahi ultramafic belt, Orissa, India. Geol. Surv. India Misc. Publ. 34 (2), 151–160.

Stowe, C.W., 1997. Chromite deposits of the Shurugwi greenstone belt, Zimbabwe. In: Stowe, C.W. (Ed.), Evolution of Chromium Ore Fields. Hutchinson Ross publication, New York, pp. 71–88.

Stowe, C.W., 1994. Compositions and tectonic settings of chromite deposits though time. Econ. Geol. 89, 528–546.

Sun, S.-S., Nesbitt, R.W., 1978. Petrogenesis of Archaean ultrabasic and basic volcanics: evidence from rare earth elements. Contrib. Mineral. Petrol. 65, 301–325.

Sun, S.-S., Nesbitt, R.W., McCulloch, M.T., 1989. Geochemistry and petrogenesis of Archaean and early Proterozoic siliceous high-magnesian basalts. In: Crawford, A.J. (Ed.), Boninites and Related Rocks. Unwin and Hyman, London, pp. 148–173.

Tesalina, S.G., Nimis, P., Augé, T., Zaykov, V.V., 2003. Origin of chromite in mafic-ultramafic-hosted hydrothermal massive sulfides from the Main Uralian Fault, South Urals, Russia. Lithos 70, 39–59.

Ulmer, G.C., 1969. Experimental investigations of chromite spinels. Econ. Geol. Monogr. 4, 114–131.

Varma, O.P., 1986. Some aspects of ultramafic and ultrabasic rocks and related chromite metallogenesis with examples from eastern region of India. In: Proceedings of the Seventy-Third Session Indian Sci. Cong. Assoc. Delhi, pp. 1–72.

Wilson, A.H., 1982. The geology of the Great 'Dyke' Zimbabwe: the ultramafic rocks. J. Petrol. 23, 240–292.

Wilson, A.H., Shirey, S.B., Carlson, R.W., 2003. Archaean ultradepleted komatiites formed by hydrous melting of cratonic mantle. Nature 423, 858–861.

Wilson, M., 1989. Igneous Petrogenesis, A Global Tectonic Approach. Chapman and Hall, London, p. 466.